JOURNAL OF COMPUTATIONAL PHYSICS **125,** 187–206 (1996)
ARTICLE NO. 0088

An Analysis of Numerical Errors in Large-Eddy Simulations of Turbulence

SANDIP GHOSAL*

Center for Turbulence Research, Stanford University, Stanford, California 94305-3030

Received August 22, 1995; revised January, 1996

The reliability of numerical simulations of turbulence depend on our ability to quantify and control discretization errors. In the classical literature on error analysis, typically, simple linear equations are studied. Estimates of errors derived from such analyses depend on the assumption that each dependent variable can be characterized by a unique amplitude and scale of spatial variation that can be normalized to unity. This assumption is not valid for strongly nonlinear problems, such as turbulence, where nonlinear interactions rapidly redistribute energy resulting in the appearance of a broad continuous spectrum of amplitudes. In such situations, the numerical error as well as the subgrid model can change with grid spacing in a complicated manner that cannot be inferred from the results of classical error analysis. In this paper, a formalism for analyzing errors in such nonlinear problems is developed in the context of finite difference approximations for the Navier–Stokes equations when the flow is fully turbulent. Analytical expressions for the power spectra of these errors are derived by exploiting the joint-normal approximation for turbulent velocity fields. These results are applied to large-eddy simulation of turbulence to obtain quantitative bounds on the magnitude of numerical errors. An assessment of the significance of these errors in made by comparing their magnitudes with that of the nonlinear and subgrid terms. One method of controlling the errors is suggested and its effectiveness evaluated through quantitative measures. Although explicit evaluations are presented only for large-eddy simulation, the expressions derived for the power spectra of errors are applicable to direct numerical simulation as well.

1. INTRODUCTION

The Navier–Stokes equations are believed to be an adequate model for the description of macroscopic motions of fluids in both the laminar as well as the turbulent regimes. Analytical solutions of these equations are known only for laminar flows. For turbulent flows one has to rely on ''direct numerical simulation'' (DNS) of the basic equations. An alternate approach that is less computationally intensive [1] is ''large-eddy simulation'' (LES). In this method, one divides the full turbulent field into a set of large-scale or ''resolved'' eddies and the small-scale or ''subgrid'' eddies. Only the resolved eddies are computed directly while the net effect of the large number of subgrid eddies is represented by a subgrid force, which is specified in a more or less ad hoc manner.

All numerical simulations of turbulence (DNS or LES) of necessity involve some numerical errors. The reliability of such simulations therefore depend on our ability to quantify and control these errors. In the classical literature (see, e.g., [2]) on analysis of errors in partial differential equations one typically studies simple linear equations (such as the wave equation or Laplace's equation). The qualitative insight gained from studying such simple situations is then used to design numerical methods for more complex problems such as Navier–Stokes turbulence. Although such an approach may seem reasonable as a first approximation, it should be recognized that strongly nonlinear problems, such as turbulence, have a feature that is absent in linear problems. This feature is the simultaneous presence of a continuum of space and time scales. Thus, in an analysis of errors in the one-dimensional wave equation, one may, without loss of generality, rescale the equations so that the dependent variable and the characteristic length scale for its fluctuations, are always of order unity. This is not possible in the turbulence problem since the amplitudes of the Fourier modes of the velocity field have a continuous distribution over a broad range of wavenumbers.

The situation is more complex in LES than in DNS. In DNS, the energy spectrum, although continuous, does decay to zero at sufficiently high wave numbers. Thus, strict control of numerical errors can always be assured by choosing a grid spacing that is much smaller than the smallest scales of motion that have significant energy. In LES, one considers only scales of motion larger than some ''filter-width'' Δ_f that are represented numerically on some grid $\Delta_g \leq \Delta_f$. The most common choice in practice is $\Delta_g = \Delta_f$. Therefore, unlike DNS, the smallest resolved scales of motion in LES still have significant energy. In this case a reasonable definition of ''acceptable level of error'' might be to require that numerical errors be small compared to the subgrid model. However, no theoretical framework for quantifying the errors in such situations exist at the present

* Present address: CNLS, Los Alamos National Laboratory, Los Alamos, NM 87545.

0021-9991/96 $18.00

time. For example, it is known from elementary error analysis that the error in a second-order finite difference scheme $\sim A\Delta^2$. However, unlike in linear problems, where $A \sim 1$ in suitable units, the amplitude A in LES would depend on Δ in a nontrivial way. The purpose of this paper is to provide a formalism with which quantitative error analysis may be carried out for such nonlinear problems.

In Section 2 the foundations of the method of analysis are developed. The solution of the discretized problem is interpreted as a vector moving in a low dimensional subspace of the full vector space of the exact solutions of the Navier–Stokes equations. A precise meaning is given to the concept of "error in a numerical method" in terms of its departure from the best solution obtainable on the subspace defined by the given grid. An exact analytical expression for the error is presented in Section 3 as the sum of "finite-differencing" and "aliasing" errors which have different origins. In Section 4, an expression for the power spectrum of the "finite-differencing" part of the error is derived. The essential tool that makes the derivation of such an analytical expression possible is the "Millionshchikov hypothesis" or the "joint-normal hypothesis" which was historically introduced into turbulence in the context of the closure problem for moment hierarchies. The essential technique is identical to that used by Batchelor in his derivation of the pressure spectrum of turbulence from the energy spectrum [3, 4]. In Section 5 a very similar analysis is used to obtain the power spectrum of the aliasing error. The power spectra of the subgrid and total nonlinear terms are computed in Section 6. These results are applied to LES of turbulence in Section 7 to obtain some quantitative measures of numerical errors in finite-difference schemes, which are increasingly being used in turbulence computations on account of their applicability to problems with complex boundaries. A discussion of these findings and quantitative evaluation of a possible method of reducing numerical errors are presented in Section 8.

2. ERRORS DUE TO SPATIAL DISCRETIZATION—FUNDAMENTALS

Turbulence of an incompressible fluid is described by the equations

$$\frac{\partial u_i}{\partial t} = -\frac{\partial}{\partial x_j}(u_i u_j) - \frac{\partial P}{\partial x_i} + \nu \nabla^2 u_i, \tag{1}$$

where the velocity (u_1, u_2, u_3) is a solenoidal vector field, and the pressure, P, is a scalar functional of the velocity field that is determined by the continuity condition. In (1) and throughout this paper the Einstein convention of summation over repeated indices is adopted unless specified otherwise. The molecular (kinematic) viscosity, ν, is positive and is constant for a given fluid. We consider the fluid to be confined in a cubical box, Ω, of side "L" and we assume periodic boundary conditions on the boundaries of Ω. The volume of the box will be denoted by $V = L^3$.

We consider a finite difference method of solving (1). In this method, the cubical domain is embedded with a rectangular grid of uniform spacing "Δ" and the velocity is defined only at the N^3 nodes of the grid that we will denote by Ω_0. Here N is the number of nodes in each direction which is assumed to be an even integer. Clearly, $\Delta = L/(N-1)$. Equations (1) are now replaced by their finite difference approximations

$$\frac{\partial u_i}{\partial t} = -\frac{\delta}{\delta x_j}(u_i u_j) - \frac{\delta P}{\delta x_i} - \frac{\delta T_{ij}^M}{\delta x_j} + \nu \frac{\delta}{\partial x_k}\frac{\delta}{\delta x_k} u_i, \tag{2}$$

where $\delta/\delta x_k$ represents a numerical differentiation scheme that approximates the continuous operator $\partial/\partial x_k$. In (2), T_{ij}^M is the discretized version of a "subgrid model" τ_{ij}^M that is specified in LES as a function (or functional) of the "u_i" and its derivatives. The subgrid model is considered to be an approximate representation of the collective effect of small-scale eddies that cannot be resolved on the LES grid. In DNS, the eddies are considered sufficiently well resolved so that the subgrid term τ_{ij}^M can be neglected. The first term on the right of (2) can be written in several alternative forms. These alternate expressions for the advective term, although equivalent in the continuum limit, result in distinct behavior of the finite discretized system. Equation (2) is known as the "divergence form" (or "conservative form"). The other most commonly used (see, e.g., [5] and references therein) discretizations are the "skew-symmetric form," "advective form" (or "non-conservative form") and "vorticity form". In this paper only the divergence form of the discretization (2) is considered for simplicity. We will also assume that the time integration of (2) is exact and suppress the time dependence of the dependent variable in our notation wherever convenient. This is done to keep the problem tractable and might be justified if time-stepping errors are negligible in comparison to errors due to finite differencing. Analysis of stability and accuracy of various temporal discretization schemes can be found in [6, 7].

Let us denote by $\mathscr{H}$ the Hilbert space consisting of the vectors $\mathbf{\Psi} = (u_1, u_2, u_3)$ whose components u_1, u_2, and u_3 are square integrable in Ω. The norm is defined as

$$\|\mathbf{\Psi} - \mathbf{\Phi}\| = \frac{1}{3}\int_\Omega d\mathbf{x}\,[(u_1 - v_1)^2 + (u_2 - v_2)^2 + (u_3 - v_3)^2], \tag{3}$$

where $\mathbf{\Psi} = (u_1, u_2, u_3)$ and $\mathbf{\Phi} = (v_1, v_2, v_3)$. The solutions

of the Navier–Stokes equations (1) can be regarded as elements of $\mathscr{H}$ and Eq. (1) can be formally written as

$$\partial_t \mathbf{\Psi} = \mathscr{N}\mathbf{\Psi}, \tag{4}$$

where $\mathscr{N}$ is a nonlinear operator defined in $\mathscr{H}$. If we define the set of wavevectors $\mathbf{k} = (2\pi n_1/L, 2\pi n_2/L, 2\pi n_3/L)$, where n_1, n_2, n_3 are integers (positive, negative, or zero), then each component of $\mathbf{\Psi}$ can be expanded in terms of the orthogonal basis functions $\exp(i\mathbf{k}\cdot\mathbf{x})$. The vectors

$$(\exp(i\mathbf{k}_1\cdot\mathbf{x}), \exp(i\mathbf{k}_2\cdot\mathbf{x}), \exp(i\mathbf{k}_3\cdot\mathbf{x})),$$

where $\mathbf{k}_1$, $\mathbf{k}_2$, and $\mathbf{k}_3$ span the set of possible wavevectors therefore form a basis $\mathscr{B}$ of $\mathscr{H}$. Any element $(u_1, u_2, u_3) \in \mathscr{H}$ can be expanded in terms of this basis as

$$u_i(\mathbf{x}) = \frac{8\pi^3}{V}\sum_{\mathbf{k}} \hat{u}_i(\mathbf{k})\exp(i\mathbf{k}\cdot\mathbf{x}), \tag{5}$$

where

$$\hat{u}_i(\mathbf{k}) = \frac{1}{8\pi^3}\int u_i(\mathbf{x})\exp(-i\mathbf{k}\cdot\mathbf{x})\, d\mathbf{x}. \tag{6}$$

In order to avoid a proliferation of subscripts, the following convention is adopted throughout this paper. Any summation over the variable $\mathbf{k}$ is assumed to run over all allowed values of $\mathbf{k}$ unless indicated otherwise in the subscript. We will ultimately pass on to the limit $L \to \infty$ at which point the summations over $\mathbf{k}$ would be replaced by integration. The domain of this integration will always be $\mathbf{R}^3$ unless otherwise indicated. All integrals with respect to the variable $\mathbf{x}$ are over Ω and all sums are over Ω_0 unless indicated otherwise. On passing to the limit $L \to \infty$ all such integrals would be in $\mathbf{R}^3$ and all summations would be over an infinite cubic lattice of spacing Δ unless a different domain is indicated in the subscript.

We would like to obtain a measure of the difference between the solutions of the approximate equations (2) and the solutions of the exact equations (1). However, the exact solution is defined in a continuous region Ω, whereas the approximate system has values only on the discrete set Ω_0. To make a comparison possible, one must first adopt some interpolation procedure to extend the values of the velocity field from the discrete set of points Ω_0 to the entire region Ω. This may be done in an infinite number of ways. For the purpose of this analysis we will choose a trigonometric interpolation, since, as will be evident later, such a choice simplifies the analytical work. In the limit of infinitely fine grid spacings, clearly, the precise choice of the interpolation method can have no effect on the final results. Further, it is not unreasonable to expect that for a finite but sufficiently fine grid the results would not be too sensitive to the nature of the interpolation. Thus, for each velocity component u_i we construct a function

$$\sum_{\mathbf{k}\in\square} c_i(\mathbf{k})\exp(i\mathbf{k}\cdot\mathbf{x}) \tag{7}$$

with the $c_i(\mathbf{k})$ chosen in such a way that (7) coincides with the computed u_i at each of the N^3 node points. In (7), $\square$ denotes the set of wavevectors whose components are in the interval $(-\pi/\Delta, +\pi/\Delta)$. It is well known [8] that such a set of coefficients can be chosen uniquely and are given by

$$c_i(\mathbf{k}) = \left(\frac{\Delta}{L}\right)^3 {\sum_{\mathbf{x}\in\Omega_0}}' u_i(\mathbf{x})\exp(-i\mathbf{k}\cdot\mathbf{x}), \tag{8}$$

where the prime over the summation sign indicates that grid points on the three planes $x = L$, $y = L$, and $z = L$ are to be excluded from the sum. Let us denote by $\mathscr{H}_0$, the subspace spanned by the basis functions with components $\exp(i\mathbf{k}\cdot\mathbf{x})$, where $\mathbf{k} \in \square$. Then it is clear from (8), that any solution on Ω_o can be extended to a vector $(u_1, u_2, u_3) \in \mathscr{H}_0$ with the expansion in terms of the basis $\mathscr{B}$ (the factors of $8\pi^3/V$ have been introduced for later convenience)

$$u_i(\mathbf{x}) = \frac{8\pi^3}{V}\sum_{\mathbf{k}} \hat{u}_i(\mathbf{k})\exp(i\mathbf{k}\cdot\mathbf{x}), \tag{9}$$

where

$$\hat{u}_i(\mathbf{k}) = \begin{cases} \dfrac{\Delta^3}{8\pi^3}{\sum_{\mathbf{x}}}' u_i(\mathbf{x})\exp(-i\mathbf{k}\cdot\mathbf{x}) & \text{if } \mathbf{k}\in\square \\ 0 & \text{otherwise.} \end{cases} \tag{10}$$

The solution of the discretized equations (2), extended from Ω_0 to Ω in the manner just described is an element of the subspace $\mathscr{H}_0$. The time evolution of this numerical solution $\mathbf{\Psi}_0$ can be formally written as

$$\partial_t \mathbf{\Psi}_0 = \mathscr{N}_0\mathbf{\Psi}_0, \tag{11}$$

where $\mathscr{N}_0$ is the "discretized Navier–Stokes operator" that maps elements of $\mathscr{H}_0$ to itself. The difference operators $\delta/\delta x_k$ in (2) are extended in $\mathscr{N}_0$ in the obvious way to act on functions defined in Ω rather than on Ω_0. Thus, for example, for a second-order central difference scheme,

$$\frac{\delta}{\delta x_1} f(\mathbf{x}) = \frac{1}{2\Delta}[f(x_1+\Delta, x_2, x_3) - f(x_1-\Delta, x_2, x_3)], \tag{12}$$

where $\mathbf{x}$ can be any point in Ω not necessarily restricted

to the nodes of the lattice and the finite-differences near boundary points are evaluated using the usual artifice of ''periodic extension'' of the domain. It is easy to prove that the effect of applying such an operator to the trigonometric extension of a function defined on a grid gives the same result as applying the difference operator first on the discrete lattice and then constructing its trigonometric extension.

The problem of designing a good numerical method can be formulated as the problem of choosing the operator $\mathcal{N}_0$ in some optimal way. Clearly, one of the objectives of any good numerical method should be to make the solution of the finite problem, $\mathbf{\Psi}_0$, as ''close'' as possible to the true solution $\mathbf{\Psi}$. Now, an element of $\mathcal{H}_0$ cannot approximate an element $\mathbf{\Psi} \in \mathcal{H}$ arbitrarily closely. However, there exists a unique element $\mathbf{\Psi}_0 \in \mathcal{H}_0$ that is closest to $\mathbf{\Psi}$ in the sense of $\|\mathbf{\Psi}_0 - \mathbf{\Psi}\|$ having the minimum possible value. The operator that maps $\mathbf{\Psi}$ to this ''closest element in $\mathcal{H}_0$'' is known [9] as the projection operator $\mathcal{P}$ corresponding to the subspace $\mathcal{H}_0$. The projection operator $\mathcal{P}$ therefore is completely determined by the subspace $\mathcal{H}_0$ and the definition of the norm $\|\ \|$. It is simple to write down an explicit expression for $\mathcal{P}$ using the basis $\mathcal{B}$,

$$\mathcal{P}(u_1, u_2, u_3) = \frac{8\pi^3}{V}\left(\sum_{\mathbf{k}\in\square} \hat{u}_1(\mathbf{k})\exp(i\mathbf{k}\cdot\mathbf{x}), \sum_{\mathbf{k}\in\square} \hat{u}_2(\mathbf{k})\exp(i\mathbf{k}\cdot\mathbf{x}), \sum_{\mathbf{k}\in\square} \hat{u}_3(\mathbf{k})\exp(i\mathbf{k}\cdot\mathbf{x})\right), \tag{13}$$

where $\hat{u}_i(\mathbf{k})$ are given by (6). This follows from the well-known result [8] that the best approximation (with respect to the L_2 norm) of a function by a finite series of trigonometric polynomials is achieved when the expansion coefficients are the Fourier coefficients. Thus, the best one can hope for from the numerical method (11) is $\mathbf{\Psi}_0 = \mathcal{P}\mathbf{\Psi}$. From (4), the equation satisfied by $\mathcal{P}\mathbf{\Psi}$ is

$$\partial_t \mathcal{P}\mathbf{\Psi} = \mathcal{P}\mathcal{N}\mathbf{\Psi}. \tag{14}$$

On subtracting (11) from (14) and adding and subtracting the term $\mathcal{N}_0\mathcal{P}\mathbf{\Psi}$ from the right-hand side, one obtains

$$\partial_t \mathbf{e} - \mathcal{N}_0\mathbf{e} = (\mathcal{P}\mathcal{N} - \mathcal{N}_0\mathcal{P})\mathbf{\Psi}, \tag{15}$$

where $\mathbf{e} \equiv \mathcal{P}\mathbf{\Psi} - \mathbf{\Psi}_0$. From (15), the necessary and sufficient condition for getting this ''best possible solution for the given grid'' is that the ''forcing term'' on the right-hand side of (15) should always be zero. This follows since the numerical solution satisfies the same boundary and initial conditions as the true solution so that $\mathbf{e}$ satisfies the corresponding ''zero'' conditions. This implies that the unique solution of (15) with a vanishing right-hand side is $\mathbf{e} = 0$. Therefore, the best possible or ideal numerical method $\mathcal{N}_0$ is one that satisfies

$$\mathcal{N}_0\mathcal{P} = \mathcal{P}\mathcal{N}. \tag{16}$$

For any $\mathbf{\Psi} \in \mathcal{H}$, we define the difference

$$\mathbf{E} \equiv (\mathcal{P}\mathcal{N} - \mathcal{N}_0\mathcal{P})\mathbf{\Psi} \tag{17}$$

as the ''error,'' that is, the extent of the departure of the solution from the best possible on the given grid. It should be noted that (17) includes errors due to the inaccuracy of the subgrid model, or ''modeling error'' as well as ''numerical errors'' that may be attributed to approximate differentiation of functions and methods of computing nonlinear terms. In Section 3, an ''ideal'' subgrid model is introduced for which there is no ''modeling error'' and the analysis in the rest of the paper is restricted to the case of such an ideal model. This is an artifice to separate issues of ''numerical errors'' from ''modeling errors'' although in reality the two effects appear together and the distinction between them is one of convention.

In the following analysis, the magnitude of the error $\mathbf{E}$ will be characterized by statistical properties such as its power spectral density. Such statistical measures can be precisely defined only in the limit, where the wavevector can assume a continuum rather than a discrete set of values. In physical space this implies that we are considering the grid size Δ and some characteristic scale of turbulence λ fixed and taking the limit as the size of the box $L \to \infty$. In actual simulations, the box size, L, is of course finite. However, L is taken much larger than Δ or λ so that smooth power spectra can be defined and computed statistical quantities are not changed when the box size is further increased. This ensures that the computed quantities are indistinguishable from the ideal limit, $L \to \infty$. For the purpose of theoretical analysis it is advantageous to take the limit $L \to \infty$ first, rather than at the end of the computation, and from now on we will assume that our lattice is infinite. Thus, in the Fourier basis, the exact solution will be characterized by the continuous family of wave vectors $\mathbf{k} \in \mathbf{R}^3$ and the numerical solution will be characterized by the subset $\mathbf{k} \in \square$, where $\square \equiv [-\pi/\Delta, \pi/\Delta] \times [-\pi/\Delta, \pi/\Delta] \times [-\pi/\Delta, \pi/\Delta]$. In the limit of infinite box size, Eqs. (5) and (6) take the form

$$u_i(\mathbf{x}) = \int \hat{u}_i(\mathbf{k})\exp(i\mathbf{k}\cdot\mathbf{x})\, d\mathbf{k} \tag{18}$$

and

$$\hat{u}_i(\mathbf{k}) = \frac{1}{8\pi^3}\int u_i(\mathbf{x})\exp(-i\mathbf{k}\cdot\mathbf{x})\, d\mathbf{x}. \tag{19}$$

For elements of $\mathscr{H}_0$, the expansions (9) and (10) take the form

$$u_i(\mathbf{x}) = \int \hat{u}_i(\mathbf{k}) \exp(i\mathbf{k}\cdot\mathbf{x})\, d\mathbf{k} \tag{20}$$

and

$$\hat{u}_i(\mathbf{k}) = \begin{cases} \dfrac{\Delta^3}{8\pi^3} \displaystyle\sum_{\mathbf{x}} u_i(\mathbf{x}) \exp(-i\mathbf{k}\cdot\mathbf{x}) & \text{if } \mathbf{k} \in \square \\ 0 & \text{otherwise.} \end{cases} \tag{21}$$

The following useful identity is also readily derived by first proving it for a finite box and then taking the limit of infinite box size,

$$\frac{\Delta^3}{8\pi^3} \sum_{\mathbf{x}} \exp(i\mathbf{K}\cdot\mathbf{x}) = \sum_{\mathbf{a}\in\Lambda} \delta(\mathbf{K} - \mathbf{a}), \tag{22}$$

where "δ" is the Dirac delta function, Λ is the set of wavevectors of the form $(2pk_m, 2qk_m, 2rk_m)$, where p, q, and r are integers (positive, negative, or zero), $k_m = \pi/\Delta$, and $\mathbf{K}$ is any vector (not necessarily restricted to $\square$). (This relation is familiar in solid state physics [10], where the set Λ goes by the name "reciprocal lattice.") Equation (22) is the discrete lattice equivalent of

$$\frac{1}{8\pi^3} \int d\mathbf{x} \exp(i\mathbf{K}\cdot\mathbf{x}) = \delta(\mathbf{K}) \tag{23}$$

and, indeed, reduces to (23) in the limit $\Delta \to 0$.

3. ERRORS DUE TO SPATIAL DISCRETIZATION—EXPLICIT FORMS AND CLASSIFICATION

In this section explicit formulae are presented for the error $\mathbf{E}$ introduced in (17). We will use the Fourier-basis $\mathscr{B}$ and denote the expansion coefficient of $\mathbf{E}$ corresponding to the wavevector $\mathbf{k}$ by $(E_1(\mathbf{k}), E_2(\mathbf{k}), E_3(\mathbf{k}))$. As explained in the last section, we consider the region Ω to be infinitely large so that the wavevector $\mathbf{k}$ may assume a continuum of values.

In order to compute $E_i(\mathbf{k})$, we first evaluate $\mathscr{P}\mathscr{N}\boldsymbol{\Psi}$ in the basis $\mathscr{B}$. Clearly, the projection operator $\mathscr{P}$ has the effect of making all Fourier coefficients corresponding to wavevectors $\mathbf{k}$ outside the region $\square$ vanish while the remaining wavevectors are unaffected. Thus,

$$\begin{aligned}(\mathscr{P}\mathscr{N}\boldsymbol{\Psi})_i(\mathbf{k}) &= H(\mathbf{k}) \Bigg[-iP_{imn}(\mathbf{k}) \int\int d\mathbf{k}'\, d\mathbf{k}'' \\ &\quad \delta(\mathbf{k}' + \mathbf{k}'' - \mathbf{k}) \hat{u}_m(\mathbf{k}') \hat{u}_n(\mathbf{k}'') - \nu k^2 \hat{u}_i(\mathbf{k}) \Bigg],\end{aligned} \tag{24}$$

where $H(\mathbf{k})$ is the unit step function defined by

$$H(\mathbf{k}) = \begin{cases} 1 & \text{if } \mathbf{k} \in \square \\ 0 & \text{otherwise.} \end{cases} \tag{25}$$

The right-hand side of (24) for $\mathbf{k} \in \square$ is simply the well-known (see, e.g., [11]) right-hand side of the Navier–Stokes equation in Fourier space. The tensor P_{imn} is defined by

$$P_{imn}(\mathbf{k}) = \begin{cases} (k_n P_{im} + k_m P_{in})/2 & \text{if } \mathbf{k} \neq 0, \\ 0 & \text{otherwise,} \end{cases} \tag{26}$$

with $P_{ij} = \delta_{ij} - k_i k_j / k^2$. It is customary to write (24) in the form

$$\begin{aligned}(\mathscr{P}\mathscr{N}\boldsymbol{\Psi})_i(\mathbf{k}) &= -iP_{imn}(\mathbf{k}) H(\mathbf{k}) \Bigg[\int_{\square}\int_{\square} d\mathbf{k}'\, d\mathbf{k}''\, \delta(\mathbf{k}' + \mathbf{k}'' \\ &\quad - \mathbf{k}) \hat{u}_m(\mathbf{k}') \hat{u}_n(\mathbf{k}'') + \hat{\tau}_{mn}(\mathbf{k}) \Bigg] \\ &\quad - \nu k^2 H(\mathbf{k}) \hat{u}_i(\mathbf{k}),\end{aligned} \tag{27}$$

where

$$\begin{aligned}\hat{\tau}_{mn}(\mathbf{k}) &= H(\mathbf{k}) \left[\int\int - \int_{\square}\int_{\square} \right] d\mathbf{k}'\, d\mathbf{k}'' \\ &\quad \hat{u}_m(\mathbf{k}') \hat{u}_n(\mathbf{k}'') \delta(\mathbf{k}' + \mathbf{k}'' - \mathbf{k})\end{aligned} \tag{28}$$

is called the subgrid stress.

Now we consider the term $\mathscr{N}_0\mathscr{P}\boldsymbol{\Psi}$. Let U_i denote the result of using the projection operator $\mathscr{P}$ on the velocity field with components u_i. Then,

$$U_i(\mathbf{x}) = \int_{\square} \hat{u}_i(\mathbf{k}) \exp(i\mathbf{k}\cdot\mathbf{x})\, d\mathbf{k}. \tag{29}$$

In the finite difference method the nonlinear term is constructed by multiplying together velocity components at each grid point. From Eqs. (20) and (21), the extension into $\mathscr{H}_0$ of such a product is $f_{mn}(\mathbf{x})$ whose Fourier coefficients are

$$\hat{f}_{mn}(\mathbf{k}) = \frac{\Delta^3}{8\pi^3} H(\mathbf{k}) \sum_{\mathbf{x}} U_m(\mathbf{x}) U_n(\mathbf{x}) \exp(-i\mathbf{k}\cdot\mathbf{x}). \tag{30}$$

When the expressions (29) for $U_i(x)$ are substituted into (30) we have

$$\hat{f}_{mn}(\mathbf{k}) = \frac{\Delta^3}{8\pi^3} H(\mathbf{k}) \sum_{\mathbf{x}} \int_{\square}\int_{\square} d\mathbf{k}'\, d\mathbf{k}'' \, \hat{u}_m(\mathbf{k}')\hat{u}_n(\mathbf{k}'')\exp[i(\mathbf{k}' + \mathbf{k}'' - \mathbf{k})\cdot\mathbf{x}]. \tag{31}$$

The summation over the lattice points can be taken inside the integral signs and executed in accordance with (22):

$$\hat{f}_{mn}(\mathbf{k}) = H(\mathbf{k}) \sum_{\mathbf{a}\in\Lambda} \int_{\square}\int_{\square} d\mathbf{k}'\, d\mathbf{k}'' \, \hat{u}_m(\mathbf{k}')\hat{u}_n(\mathbf{k}'')\delta(\mathbf{k}' + \mathbf{k}'' - \mathbf{k} - \mathbf{a}). \tag{32}$$

Thus, $\mathscr{N}_0\mathscr{P}\boldsymbol{\Psi}$ differs from $\mathscr{P}\mathscr{N}\boldsymbol{\Psi}$ in that the expression (32) replaces the nonlinear term

$$H(\mathbf{k}) \int\int d\mathbf{k}'\, d\mathbf{k}''\, \delta(\mathbf{k}' + \mathbf{k}'' - \mathbf{k})\hat{u}_m(\mathbf{k}')\hat{u}_n(\mathbf{k}'')$$

in Eq. (24). Further, all expressions involving the wavevectors $\mathbf{k}$ in (24) should be replaced by the corresponding modified wavevectors $\tilde{\mathbf{k}}$. The "modified wavevector" is simply the numerical differentiation operator expressed in Fourier space [12]. If the exact derivative operator $\partial/\partial x_k$ is replaced by the numerical differentiation $\delta/\delta x_k$, multiplication by wavevectors $\mathbf{k}$ in Fourier space are replaced by multiplication by the corresponding modified wavevectors $\tilde{\mathbf{k}}$.

In order to complete the evaluation of $\mathscr{N}_0\mathscr{P}$ we need an explicit specification of the subgrid model τ_{ij}^M. Any subgrid model introduces into the problem the "subgrid modeling error" $\tau_{ij} - \tau_{ij}^M$. This makes further quantitative analysis impossible since at the present state of turbulence theory, all subgrid models are ad hoc uncontrolled approximations and it is impossible to put any rigorous quantitative bounds on the subgrid modeling error. Although numerical errors associated with spatial discretization of a given subgrid model may be computed there is no obvious way to single out for this study any one among the wide variety of subgrid models in use. In order to avoid such complications, we introduce the concept of the "ideal subgrid model"

$$\tau_{ij}^M = \tau_{ij}(\mathbf{x}, t), \tag{33}$$

where $\tau_{ij}(\mathbf{x}, t)$ is the exact subgrid stress whose Fourier coefficients are defined in (28). One might think of the "ideal subgrid model" (33) in the following way. Imagine a DNS with an infinitely greater resolution running concurrently with the given LES. At every time-step the exact subgrid stress is computed from the DNS field and supplied to the LES simulation as a function of position. The rest of the analysis in this paper will be presented for such an idealized LES. Since τ_{ij}^M is already given as a function of position and time and involves no computation, and since it has no components outside $\square$,

$$T_{ij}^M = \tau_{ij}^M = \tau_{ij}(\mathbf{x}, t). \tag{34}$$

Now we can write down the expression for $\mathscr{N}_0\mathscr{P}\boldsymbol{\Psi}$:

$$(\mathscr{N}_0\mathscr{P}\boldsymbol{\Psi})_i(\mathbf{k}) = -iP_{imn}(\tilde{\mathbf{k}})H(\mathbf{k})\Bigg[\sum_{\mathbf{a}\in\Lambda}\int_{\square}\int_{\square} d\mathbf{k}'\, d\mathbf{k}''\, \delta(\mathbf{k}' + \mathbf{k}'' - \mathbf{k} - \mathbf{a})\hat{u}_m(\mathbf{k}')\hat{u}_n(\mathbf{k}'') + \hat{\tau}_{mn}(\mathbf{k})\Bigg] - \nu\tilde{k}^2 H(\mathbf{k})\hat{u}_i(\mathbf{k}) \tag{35}$$

On taking the difference of (24) and (35) we observe that the error may be written as

$$E_i(\mathbf{k}) = E_i^{(\mathrm{FD})}(\mathbf{k}) + E_i^{(\mathrm{alias})}(\mathbf{k}), \tag{36}$$

where

$$\begin{aligned} E_i^{(\mathrm{FD})}(\mathbf{k}) &= iH(\mathbf{k})[P_{imn}(\tilde{\mathbf{k}}) - P_{imn}(\mathbf{k})]\Bigg[\int_{\square}\int_{\square} d\mathbf{k}'\, d\mathbf{k}'' \\ &\quad \delta(\mathbf{k}' + \mathbf{k}'' - \mathbf{k})\hat{u}_m(\mathbf{k}')\hat{u}_n(\mathbf{k}'') + \hat{\tau}_{mn}(\mathbf{k})\Bigg] \\ &\quad + \nu(\tilde{k}^2 - k^2)H(\mathbf{k})\hat{u}_i(\mathbf{k}) \\ &= iH(\mathbf{k})[P_{imn}(\tilde{\mathbf{k}}) - P_{imn}(\mathbf{k})]\Bigg[\int\int d\mathbf{k}'\, d\mathbf{k}'' \\ &\quad \delta(\mathbf{k}' + \mathbf{k}'' - \mathbf{k})\hat{u}_m(\mathbf{k}')\hat{u}_n(\mathbf{k}'')\Bigg] \\ &\quad + \nu(\tilde{k}^2 - k^2)H(\mathbf{k})\hat{u}_i(\mathbf{k}) \end{aligned} \tag{37}$$

and

$$E_i^{(\mathrm{alias})}(\mathbf{k}) = iP_{imn}(\tilde{\mathbf{k}})H(\mathbf{k}) \sum_{\mathbf{a}\in\Lambda_0} \int_{\square}\int_{\square} d\mathbf{k}'\, d\mathbf{k}'' \, \delta(\mathbf{k}' + \mathbf{k}'' - \mathbf{k} - \mathbf{a})\hat{u}_m(\mathbf{k}')\hat{u}_n(\mathbf{k}''). \tag{38}$$

In (38), the "reciprocal lattice" Λ was replaced by the smaller set Λ_0 consisting of the vectors $(2pk_m, 2qk_m, 2rk_m)$, where p, q, and r can independently take on the values 0

or ± 1 but excluding the case $p = q = r = 0$. The reason integer values of p, q, and r with modulus greater than 1 are not included in Λ_0 is that the relation $\mathbf{a} = \mathbf{k}' + \mathbf{k}'' - \mathbf{k}$ cannot be satisfied for such values if $\mathbf{k}, \mathbf{k}', \mathbf{k}'' \in \square$ and, hence, the delta function ensures that they do not contribute to the sum. The first term in (36) arises because of the inability of the finite-differencing operator, $\delta/\delta x_k$, to accurately compute the gradient of short-wavelength waves. We call this the "finite-differencing error." It vanishes for a spectral method which can differentiate waves of all wavelengths exactly. The second term arises due to the method of computation of the nonlinear term by taking products in physical space on a discrete lattice. This is called the "aliasing error" and is well known in the literature on pseudo-spectral methods [13, 14].

4. FINITE-DIFFERENCING ERRORS

In this section, an expression for the power spectrum of finite-differencing errors is obtained analytically. The power spectrum of the finite-differencing error is defined by $\mathscr{E}^{(\mathrm{FD})}(k)$, where

$$\frac{\mathscr{E}^{(\mathrm{FD})}(k)}{4\pi k^2} = \lim_{V\to\infty} \frac{8\pi^3}{V} \{\langle E_i^{(\mathrm{FD})}(\mathbf{k}) E_i^{(\mathrm{FD})}(\mathbf{k})^* \rangle\}_\Omega, \qquad (39)$$

$\{\}_\Omega$ denotes angular average in wave-number space over the surface of the sphere $|\mathbf{k}| = k$ and V is the volume of the physical box containing the fluid. The prefactor $8\pi^3/V$ in (39) is necessary because we would like the integral of the power spectra over the entire region $\square$ to give us the mean-square error rather than the square of the error summed over the infinite lattice (which of course would be infinite!). The appearance of the volume "V" of the box at this stage of the calculation may at first sight seem surprising since we have been working with an infinite lattice all along. The intent of (39) is that the entire calculation within the "$\{\}_\Omega$" should first be done in the finite box, the result multiplied by $8\pi^3/V$, and the limit $V \to \infty$ taken as the final step. However, it is easier to work directly with an infinite lattice from the start. This formal procedure is correct provided the "leftover δ-functions" from the calculation within the "$\{\}_\Omega$" are handled in the following way: the combination $8\pi^3\delta(\mathbf{k})/V$ is to be interpreted as the "Kronecker-delta" symbol $\delta_\mathbf{k}$ (defined as 1 if $\mathbf{k} = 0$ and 0 otherwise) in accordance with the familiar rule $(V/8\pi^3)\delta_\mathbf{k} \to \delta(\mathbf{k})$ for passing to the continuum limit. The difference between the two methods is only formal and the same result is obtained by working with a finite lattice and taking the limit $V \to \infty$ at the final step.

From (37), we have, for $\mathbf{k} \in \square$,

$$\begin{aligned}
&\langle E_i^{\mathrm{FD}}(\mathbf{k}) E_i^{\mathrm{FD}}(\mathbf{k})^* \rangle \\
&\quad = \Delta_{imn}(\mathbf{k}, \tilde{\mathbf{k}}) \Delta^*_{ipq}(\mathbf{k}, \tilde{\mathbf{k}}) \int\int d\mathbf{k}'\, d\mathbf{k}'' \\
&\qquad \langle \hat{u}_m(\mathbf{k}') \hat{u}_n(\mathbf{k} - \mathbf{k}') \hat{u}_p^*(\mathbf{k}'') \hat{u}_q^*(\mathbf{k} - \mathbf{k}'') \rangle \\
&\qquad + 2\nu \Im \left[i \Delta^*_{imn}(\mathbf{k}, \tilde{\mathbf{k}}) (\tilde{k}^2 - k^2) \int d\mathbf{k}' \right. \\
&\qquad \left. \langle \hat{u}_m^*(\mathbf{k}') \hat{u}_n^*(\mathbf{k} - \mathbf{k}') \hat{u}_i(\mathbf{k}) \rangle \right] \\
&\qquad + \nu^2 |\tilde{k}^2 - k^2|^2 \langle \hat{u}_i(\mathbf{k}) \hat{u}_i^*(\mathbf{k}) \rangle,
\end{aligned} \qquad (40)$$

where $\langle\ \rangle$ denotes ensemble average, * denotes complex conjugate, $\Im$ denotes the imaginary part, and $\Delta_{imn}(\mathbf{k}, \tilde{\mathbf{k}}) \equiv P_{imn}(\tilde{\mathbf{k}}) - P_{imn}(\mathbf{k})$. The following two properties of the Δ_{imn} tensors follow immediately from the corresponding properties of P_{imn}; $\Delta_{imn} = 0$, $\Delta_{imn} = \Delta_{inm}$.

In order to make further analytical work possible with (40) we now introduce the "Millionshchikov hypothesis" [15] that in fully developed turbulence, the joint probability density function of any set of velocity components at arbitrary space-time points can be assumed to be joint-normal. The joint-normal hypothesis was originally evoked in turbulence in an attempt to close the hierarchy of equations for moments [11]. Although this did not succeed, the joint-normal hypothesis has been successfully used in other contexts. Thus, Batchelor [3] used it with success to predict the pressure spectrum of isotropic turbulence. A detailed discussion of the joint normal hypothesis may be found in [15]. The joint-normal hypothesis implies, in particular,

$$\begin{aligned}
\langle u_i(\mathbf{x}_1) u_j(\mathbf{x}_2) u_k(\mathbf{x}_3) u_l(\mathbf{x}_4) \rangle &= \langle u_i(\mathbf{x}_1) u_j(\mathbf{x}_2) \rangle \langle u_k(\mathbf{x}_3) u_l(\mathbf{x}_4) \rangle \\
&\quad + \langle u_i(\mathbf{x}_1) u_k(\mathbf{x}_3) \rangle \langle u_j(\mathbf{x}_2) u_l(\mathbf{x}_4) \rangle \\
&\quad + \langle u_i(\mathbf{x}_1) u_l(\mathbf{x}_4) \rangle \langle u_j(\mathbf{x}_2) u_k(\mathbf{x}_3) \rangle
\end{aligned} \qquad (41)$$

and that all third-order moments are zero. Here $\mathbf{u}(\mathbf{x}, t)$ is the true velocity field defined at all space time points. On taking the Fourier transform (in infinite continuous space) of (41) and assuming the turbulence to be homogeneous, we have

$$\begin{aligned}
&\langle \hat{u}_i(\mathbf{k}_1) \hat{u}_j(\mathbf{k}_2) \hat{u}_k(\mathbf{k}_3) \hat{u}_l(\mathbf{k}_4) \rangle \\
&\quad = \delta(\mathbf{k}_1 + \mathbf{k}_2) \delta(\mathbf{k}_3 + \mathbf{k}_4) \Phi_{ij}(\mathbf{k}_2) \Phi_{kl}(\mathbf{k}_4) \\
&\qquad + \delta(\mathbf{k}_1 + \mathbf{k}_3) \delta(\mathbf{k}_2 + \mathbf{k}_4) \Phi_{ik}(\mathbf{k}_3) \Phi_{jl}(\mathbf{k}_4) \\
&\qquad + \delta(\mathbf{k}_1 + \mathbf{k}_4) \delta(\mathbf{k}_2 + \mathbf{k}_3) \Phi_{il}(\mathbf{k}_4) \Phi_{jk}(\mathbf{k}_3),
\end{aligned} \qquad (42)$$

where Φ_{ij} is the Fourier transform of the correlation tensor $R_{ij}(\mathbf{x}_2 - \mathbf{x}_1) \equiv \langle u_i(\mathbf{x}_1) u_j(\mathbf{x}_2) \rangle$. On substituting (42) into the

first term in (40) we get a sum of three terms. It is readily seen that the first of these three terms is proportional to $\delta(\mathbf{k})$ which when combined with $8\pi^3/V$ from (39) gets replaced by $\delta_{\mathbf{k}}$. Since $\Delta_{ipq}(\mathbf{k}, \tilde{\boldsymbol{k}})$ vanishes if $\mathbf{k} = 0$, there is no contribution from this term. Further, since $\Delta_{ipq}(\mathbf{k}, \tilde{\mathbf{k}})$ is invariant with respect to an interchange of the last two indices, the second and third terms are equal. Thus, the total contribution is

$$2\Delta_{imn}(\mathbf{k}, \tilde{\mathbf{k}})\, \Delta^*_{ipq}(\mathbf{k}, \tilde{\mathbf{k}}) \int d\mathbf{k}'\, \Phi^*_{mp}(\mathbf{k}')\Phi^*_{nq}(\mathbf{k} - \mathbf{k}'), \tag{43}$$

where the factor $8\pi^3\, \delta(0)/V$ has been replaced with $\delta_0 = 1$ in accordance with the procedure for taking the limit explained earlier. The second term of (40) vanishes under the joint-normal hypothesis and the last term is easily shown to be

$$\frac{\int d\mathbf{x}}{8\pi^3}\, \nu^2|\tilde{k}^2 - k^2|^2\Phi_{ii}. \tag{44}$$

The first factor is eliminated by the $8\pi^3/V$ in (39) and we obtain finally

$$\begin{aligned}\mathscr{E}^{(\mathrm{FD})}(k) &= \Big\{8\pi k^2\, \Delta_{imn}(\mathbf{k}, \tilde{\mathbf{k}})\, \Delta^*_{ipq}(\mathbf{k}, \tilde{\mathbf{k}}) \int \Phi^*_{mp}(\mathbf{k}') \\ &\quad \Phi^*_{nq}(\mathbf{k} - \mathbf{k}')\, d\mathbf{k}' + 4\pi k^2\nu^2|\tilde{k}^2 - k^2|^2\Phi_{ii}(\mathbf{k})\Big\}_\Omega.\end{aligned} \tag{45}$$

Equation (45) is the general result for homogeneous turbulence. If in addition, the turbulence is isotropic, Φ_{ij} simplifies [4] to

$$\Phi_{ij}(\mathbf{k}) = \frac{E(k)}{4\pi k^4}(k^2\, \delta_{ij} - k_i k_j), \tag{46}$$

where $E(k)$ is the three-dimensional energy spectrum and δ_{ij} is the Kronecker-delta symbol. The integral in the first term of (45) may be written after substitution of (46) as

$$\begin{aligned}J_{mpnq}(\mathbf{k}) &\equiv 8\pi k^2 \int \Phi^*_{mp}(\mathbf{k}')\Phi^*_{nq}(\mathbf{k} - \mathbf{k}')\, d\mathbf{k}' \\ &= \frac{k^2}{2\pi}\int\int \frac{E(P)E(Q)}{P^4Q^4}[P^2Q^2\, \delta_{mp}\, \delta_{nq} \\ &\quad - P_m P_p Q^2\, \delta_{nq} - Q_n Q_q P^2\, \delta_{mp} \\ &\quad + P_m P_p Q_n Q_q]\delta(\mathbf{P} + \mathbf{Q} - \mathbf{k})\, d\mathbf{P}\, d\mathbf{Q}.\end{aligned} \tag{47}$$

This integral is evaluated in the Appendix. The result is

$$\begin{aligned}J_{mpnq}(\mathbf{k}) &= F_1(k)\, \delta_{mp}\, \delta_{nq} + F_2(k)(\delta_{mn}\, \delta_{pq} + \delta_{pn}\, \delta_{mq}) \\ &\quad + F_3(k)\left[\frac{k_m k_p}{k^2}\, \delta_{nq} + \frac{k_n k_q}{k^2}\, \delta_{mp}\right] \\ &\quad + F_4(k)\frac{k_m k_p k_n k_q}{k^4},\end{aligned} \tag{48}$$

where

$$F_1(k) = \tfrac{1}{16}[7I_4 + 6I_3 - 2I_2 + 5I_1] \tag{49}$$

$$F_2(k) = \tfrac{1}{16}[-3I_4 + 2I_3 + 2I_2 - I_1] \tag{50}$$

$$F_3(k) = \tfrac{1}{16}[-15I_4 - 6I_3 + 2I_2 + 3I_1] \tag{51}$$

$$F_4(k) = \tfrac{1}{16}[45I_4 - 30I_3 - 6I_2 + 7I_1]. \tag{52}$$

The terms I_m are defined as

$$I_m = k\int_0^\infty d\xi \int_{|\xi-1|}^{\xi+1} d\eta\, E(k\xi)E(k\eta)W_m(\xi, \eta), \tag{53}$$

where the weights W_m are defined as

$$W_1(\xi, \eta) = \frac{1}{\xi\eta} \tag{54}$$

$$W_2(\xi, \eta) = \frac{(1 - \xi^2 - \eta^2)^2}{4\xi^3\eta^3} \tag{55}$$

$$W_3(\xi, \eta) = \frac{(1 + \xi^2 - \eta^2)^2}{4\xi^3\eta} \tag{56}$$

$$W_4(\xi, \eta) = \frac{[1 - (\xi^2 - \eta^2)^2]^2}{16\xi^3\eta^3}. \tag{57}$$

Therefore, after substituting (48) in (45) and using the properties $\Delta_{imm} = 0$ and $\Delta_{imn} = \Delta_{inm}$, the following expression is obtained for the power spectrum of the finite-differencing error (no summation over repeated indices !):

$$\begin{aligned}\mathscr{E}^{(\mathrm{FD})}(k) &= [F_1(k) + F_2(k)]\Big\{\sum_{i,m,n}|\Delta_{imn}(\mathbf{k}, \tilde{\mathbf{k}})|^2\Big\}_\Omega \\ &\quad + 2F_3(k)\Big\{\sum_{i,m,n,p}\frac{k_m k_p}{k^2}\Delta_{imn}(\mathbf{k}, \tilde{\mathbf{k}})\, \Delta^*_{ipn}(\mathbf{k}, \tilde{\mathbf{k}})\Big\}_\Omega \\ &\quad + F_4(k)\Big\{\sum_{i,m,n,p,q}\frac{k_m k_p k_n k_q}{k^4}\Delta_{imn}(\mathbf{k}, \tilde{\mathbf{k}})\, \Delta^*_{ipq}(\mathbf{k}, \tilde{\mathbf{k}})\Big\}_\Omega \\ &\quad + 2\nu^2 E(k)\{|\tilde{k}^2 - k^2|^2\}_\Omega.\end{aligned} \tag{58}$$

In Eq. (58), the functions $F_1(k)$, $F_2(k)$, $F_3(k)$, and $F_4(k)$ are known once the energy spectrum is specified. They are

not affected by the choice of numerical schemes. On the other hand, the coefficients of these functions in (58) depend *only* on the numerical method (through the dependence of $\tilde{\mathbf{k}}$ on $\mathbf{k}$) and are quite independent of the physical spectrum. Thus, given a specific numerical scheme and energy spectrum, Eq. (58) can be used to compute the power spectrum of the finite-differencing error. This is done in Section 7 for various representative numerical schemes.

5. ALIASING ERRORS

In this section, an analytical expression for the power spectrum of the aliasing-error is derived. The power spectrum of the aliasing error, $\mathscr{E}^{(\text{alias})}(k)$, is given by

$$\frac{\mathscr{E}^{(\text{alias})}(k)}{4\pi k^2} = \lim_{V\to\infty} \frac{8\pi^3}{V} \{\langle E_i^{(\text{alias})}(\mathbf{k}) E_i^{(\text{alias})}(\mathbf{k})^*\rangle\}_\Omega, \quad (59)$$

where the meaning of the limit operation was as explained in the last section. From (38) one obtains, for $\mathbf{k} \in \square$,

$$\begin{aligned}\langle E_i^{\text{alias}}(\mathbf{k}) E_i^{\text{alias}}(\mathbf{k})^*\rangle &= P_{imn}(\tilde{\mathbf{k}}) P_{ipq}^*(\tilde{\mathbf{k}}) \\ &\sum_{\mathbf{a},\mathbf{a}'\in\Lambda_0} \int_\square \int_\square \int_\square \int_\square d\mathbf{k}_1\, d\mathbf{k}_2\, d\mathbf{k}_3\, d\mathbf{k}_4 \\ &\langle \hat{u}_m(\mathbf{k}_1)\hat{u}_n(\mathbf{k}_2)\hat{u}_p^*(\mathbf{k}_3)\hat{u}_q^*(\mathbf{k}_4)\rangle \\ &\delta(\mathbf{k}+\mathbf{a}-\mathbf{k}_1-\mathbf{k}_2)\,\delta(\mathbf{k}+\mathbf{a}'-\mathbf{k}_3-\mathbf{k}_4).\end{aligned} \quad (60)$$

On applying the joint-normal hypothesis, in analogy to the derivation of (58), one gets

$$\begin{aligned}\lim_{V\to\infty} \frac{8\pi^3}{V} \langle E_i^{\text{alias}}(\mathbf{k}) E_i^{\text{alias}}(\mathbf{k})^*\rangle &= 2 \sum_{\mathbf{a}\in\Lambda_0} \\ P_{imn}(\tilde{\mathbf{k}}) P_{ipq}^*(\tilde{\mathbf{k}}) &\int_\square \int_\square d\mathbf{k}'\, d\mathbf{k}'' \\ \delta(\mathbf{k}'+\mathbf{k}''-\mathbf{k}-\mathbf{a})&\Phi_{mp}^*(\mathbf{k}')\Phi_{nq}^*(\mathbf{k}'').\end{aligned} \quad (61)$$

Here the factor $8\pi^3\,\delta(\mathbf{a}-\mathbf{a}')/V$ was replaced by $\delta_{\mathbf{a}-\mathbf{a}'}$ in accordance with the procedure explained in the last section. Thus,

$$\begin{aligned}\mathscr{E}^{(\text{alias})}(k) = 8\pi k^2 \sum_{\mathbf{a}\in\Lambda_0} \Big\{ &P_{imn}(\tilde{\mathbf{k}}) P_{ipq}^*(\tilde{\mathbf{k}}) \int_\square \int_\square \\ &d\mathbf{k}'\, d\mathbf{k}''\, \Phi_{mp}^*(\mathbf{k}')\Phi_{nq}^*(\mathbf{k}'')\,\delta(\mathbf{k}+\mathbf{a}-\mathbf{k}'-\mathbf{k}'')\Big\}_\Omega.\end{aligned} \quad (62)$$

The integral in (62) is difficult to handle analytically because integration over the cubical region $\square$ destroys the spherical symmetry of the problem that was exploited in the computation of J_{mpnq} in the last section. In order to make analytical progress, the following approximation is introduced. The region $\square$, which is a cube in $\mathbf{k}$-space, is replaced by the largest sphere contained in it. Clearly, this procedure can be implemented simply by removing the suffix "$\square$" from the integral signs in (62) and replacing the energy spectrum $E(k)$ by

$$E^{\min}(k) = \begin{cases} E(k) & \text{if } k < k_m \\ 0 & \text{otherwise.}\end{cases} \quad (63)$$

The superscript "min" indicates that this procedure underestimates the true aliasing error by failing to take account of the contribution of modes close to the eight corners of the cube. An alternative method that overestimates the error can be provided by replacing the cube by the smallest sphere that contains it. To obtain this estimate one needs to use in place of $E^{\min}$ the following spectrum:

$$E^{\max}(k) = \begin{cases} E(k) & \text{if } k < \sqrt{3}k_m \\ 0 & \text{otherwise.}\end{cases} \quad (64)$$

The true aliasing error is then expected to lie between these two bounds. (However, a rigorous mathematical proof of this fact based directly on the formula (62) has not been found, although the result seems very plausible.) With the approximation so described, the integral in (62) may be extended to the entire wave space. Thus, one obtains

$$\mathscr{E}^{(\text{alias})}(k) = \sum_{\mathbf{a}\in\Lambda_0} \{P_{imn}(\tilde{\mathbf{k}}) P_{ipq}^*(\tilde{\mathbf{k}}) J_{mpnq}(\mathbf{k}+\mathbf{a})\}_\Omega. \quad (65)$$

Substitution of the expression for J_{mpnq} from the Appendix gives (no summation over repeated indices !)

$$\begin{aligned}\mathscr{E}^{(\text{alias})}(k) = \sum_{\mathbf{a}\in\Lambda_0} \Big\{ &[F_1(K)+F_2(K)] \sum_{i,m,n} |P_{imn}(\tilde{\mathbf{k}})|^2 \\ &+ 2F_3(K) \sum_{i,m,n,p} \frac{K_m K_p}{K^2} P_{imn}(\tilde{\mathbf{k}}) P_{ipn}^*(\tilde{\mathbf{k}}) \\ &+ F_4(K) \sum_{i,m,n,p,q} \frac{K_m K_p K_n K_q}{K^4} P_{imn}(\tilde{\mathbf{k}}) P_{ipq}^*(\tilde{\mathbf{k}}) \Big\}_\Omega,\end{aligned} \quad (66)$$

where $\mathbf{K} = \mathbf{k} + \mathbf{a}$. Note that in this case the $F_i(K)$ does depend on the direction of $\mathbf{k}$ so that the $F_i(K)$ cannot be extracted from the $\{\ \}_\Omega$ operation. Although the summation over the set Λ_0 consists of $3^3 - 1 = 26$ terms, for a cubical box one only needs to evaluate three terms due to symmetry. Indeed, the full set of "aliasing modes," $\mathbf{a} \in \Lambda_0$, fall into three classes [14]:

$$3D\{(\pm 2k_m, \pm 2k_m, \pm 2k_m), \quad 2D\begin{cases}(\pm 2k_m, \pm 2k_m, 0)\\ (\pm 2k_m, 0, \pm 2k_m),\\ (0, \pm 2k_m, \pm 2k_m)\end{cases} \quad 1D\begin{cases}(\pm 2k_m, 0, 0)\\ (0, \pm 2k_m, 0)\\ (0, 0, \pm 2k_m).\end{cases} \tag{67}$$

By symmetry all the contributions within each class are equal. Therefore,

$$\mathscr{E}^{(\text{alias})}(k) = 6\,\mathscr{E}_{1D}^{(\text{alias})}(k) + 12\,\mathscr{E}_{2D}^{(\text{alias})}(k) + 8\,\mathscr{E}_{3D}^{(\text{alias})}(k), \tag{68}$$

where $\mathscr{E}_{1D}^{(\text{alias})}(k)$ is the contribution from any one of the 1D modes, $\mathscr{E}_{2D}^{(\text{alias})}(k)$ is the contribution from any one of the 2D modes, and $\mathscr{E}_{3D}^{(\text{alias})}(k)$ is the contribution from any one of the 3D modes, respectively. If the modified wavevector $\tilde{\mathbf{k}}$ of a numerical method and the energy spectrum of the turbulence, $E(k)$ are known, (66) may be evaluated numerically using either $E^{\min}(k)$ or $E^{\max}(k)$ (defined in (63) and (64)) to get the lower or upper bound for the aliasing error, respectively.

6. SUBGRID AND TOTAL CONTRIBUTIONS

In this section, the power spectrum of the exact subgrid force and the total nonlinear term will be computed. This information will be used in the following sections as a benchmark to evaluate numerical errors in LES. The total nonlinear term **N** and the (exact) subgrid force **S** can be readily written down in terms of the Fourier basis:

$$N_i(\mathbf{k}) = -iP_{imn}(\mathbf{k}) \int\int d\mathbf{k}'\, d\mathbf{k}''\, \delta(\mathbf{k}' + \mathbf{k}'' - \mathbf{k})\hat{u}_m(\mathbf{k}')\hat{u}_n(\mathbf{k}'') \tag{69}$$

and

$$S_i(\mathbf{k}) = -iP_{imn}(\mathbf{k})H(\mathbf{k}) \left(\int\int - \int_{\square}\int_{\square}\right) d\mathbf{k}'\, d\mathbf{k}''\, \delta(\mathbf{k}' + \mathbf{k}'' - \mathbf{k})\hat{u}_m(\mathbf{k}')\hat{u}_n(\mathbf{k}''). \tag{70}$$

The power spectra are defined as

$$\frac{\mathscr{S}(k)}{4\pi k^2} = \lim_{V\to\infty} \frac{8\pi^3}{V}\{\langle S_i(\mathbf{k})S_i(\mathbf{k})^*\rangle\}_\Omega \tag{71}$$

$$\frac{\mathscr{N}(k)}{4\pi k^2} = \lim_{V\to\infty} \frac{8\pi^3}{V}\{\langle N_i(\mathbf{k})N_i(\mathbf{k})^*\rangle\}_\Omega, \tag{72}$$

where $\{\}_\Omega$ as usual denotes angular average over the sphere $|\mathbf{k}| = k$.

The evaluation of (72) is similar to the calculation of $\mathscr{E}^{\text{FD}}(k)$ in Section 4. One only needs to replace "Δ_{imn}" in (58) by "$-P_{imn}$" and drop the last term involving the viscosity. The resulting expressions can be further simplified using the following properties of the P_{imn} tensor:

$$P_{imn}P_{imn} = k^2, \tag{73}$$

$$k_m k_p P_{imn} P_{ipn} = \frac{1}{4}k^4 P_{in}P_{in} = \frac{k^4}{2}, \tag{74}$$

$$k_m k_n P_{imn} = 0. \tag{75}$$

Thus,

$$\mathscr{N}(k) = k^2[F_1(k) + F_2(k) + F_3(k)], \tag{76}$$

where $F_1(k)$, $F_2(k)$, and $F_3(k)$ are as defined in Section 4.

The computation of $\mathscr{S}(k)$ once again requires us to restrict the **k** space integration to a cubical domain which makes it difficult to handle the integrals analytically. This difficulty is dealt with in precisely the same manner as was done in the computation of the aliasing error. The cubical domain in **k** space is replaced by a spherical region of appropriate size. This is completely equivalent to replacing the energy spectrum $E(k)$ by a pseudo-spectrum as in Section 5. With this modification, the calculation is exactly identical to that just presented for the nonlinear term. Thus, one obtains

$$\mathscr{S}(k) = k^2[F_1(k) + F_2(k) + F_3(k)], \tag{77}$$

where in the evaluation of the functions F_i, the "pseudo-spectrum"

$$E^{\min}(k) = \begin{cases}0 & \text{if } k < \sqrt{3}k_m\\ E(k) & \text{otherwise,}\end{cases} \tag{78}$$

or

$$E^{\max}(k) = \begin{cases}0 & \text{if } k < k_m\\ E(k) & \text{otherwise,}\end{cases} \tag{79}$$

should be used in place of $E(k)$ to obtain the lower and upper bounds, respectively.

7. LARGE-EDDY SIMULATION

The results established in the previous sections will now be applied to derive quantitative measures of errors in large-eddy simulation. In large-eddy simulation the grid

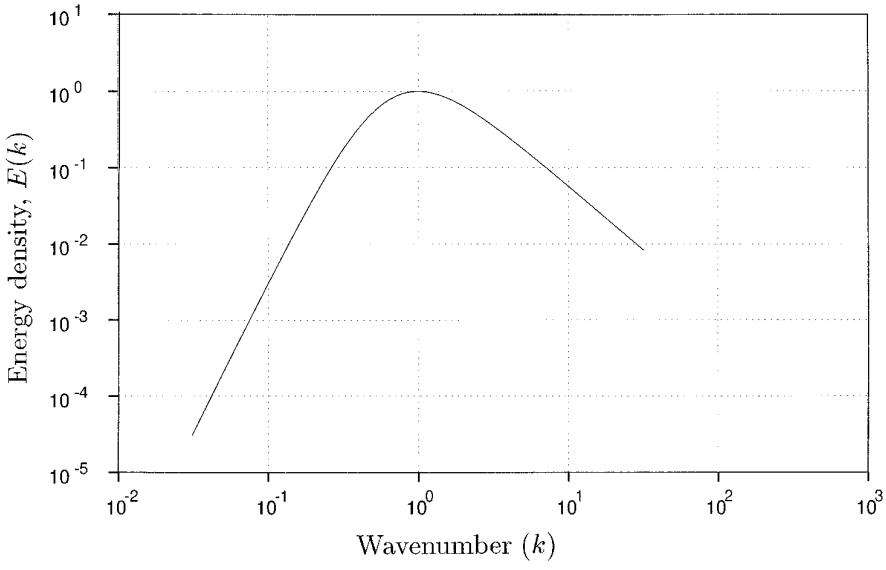

FIG. 1. The Von-Karman spectrum normalized so that the maximum energy density is at $k = 1$ and $E(1) = 1$.

spacing Δ is typically much larger than the Kolmogorov length so that molecular viscosity plays a negligible role. Therefore "ν" is set to zero throughout this section. For the energy spectrum we assume the "Von-Karman form"

$$E(k) = \frac{ak^4}{(b + k^2)^{17/6}}, \tag{80}$$

where the constants $a = 2.682$ and $b = 0.417$ are chosen so that the maximum of $E(k)$ occurs at $k = 1$ and the maximum value $E(1) = 1$. This can always be ensured by a proper choice of length and time scales. The Von-Karman spectrum has the property $E(\mathrm{k}) \sim k^4$ as $k \to 0$ and $E(k) \sim k^{-5/3}$ as $k \to \infty$ and is a fair representation of inertial range turbulence. A plot of this spectrum is shown in Fig. 1.

7.1. *Spectra*

The power spectra $\mathcal{N}(k)$ and $\mathcal{I}(k)$ are evaluated numerically from (76) and (77), respectively, using the Von-Karman spectrum. The results are shown in Fig. 2 for $k_m = 8$ and 32. It is seen that the power spectrum of the total nonlinear term is reasonably flat at high wavenumbers while the subgrid contribution raises monotonically to a maximum (which appears as a "cusp" when plotted on a linear scale) at the cutoff wavenumber k_m. The subgrid contribution is seen to be a relatively small part of the total conbribution from the nonlinear term.

Subgrid modeling is a very important part of large-eddy simulation. A parametrization of the interacton of the unresolved eddies with the resolved onces is expressed as a subgrid model. It is therefore desirable that the errors inherent in the numerical method be much smaller than the physically motivated subgrid model. We now examine to what extent such an expectation is realized for a second-order central-difference method implemented with the nonlinear term in divergence form. A second-order central-difference scheme is characterized by the modified wavenumber $\tilde{k}_i = \sin(k_i\Delta)/\Delta$ ($i = 1$, 2, or 3). Equation (58) is used to compute the power spectrum of the finite-differencing error $\mathscr{E}^{(\mathrm{FD})}(k)$. These results are compared to the power spectra of the respective subgrid terms in Fig. 3 for $k_m = 8$ and 32. They have the same qualitative appearance for other values of k_m. The power spectrum of the finite-differencing error also rises to a maximum at $k = k_m$ in the same manner as the subgrid contribution. However, the finite-differencing error is substantially larger than the subgrid contribution over the entire wavenumber range.

Figure 3 indicates that the error in a low order scheme cannot be reduced to an acceptable level by sufficiently refining the grid. This is because as the grid is refined (k_m is increased) the subgrid contribution also decreases such that the error dominates the subgrid contribution irrespective of the resolution. Let us now examine if this situation can be improved by using higher order central-difference schemes. Figure 4 shows the finite-differencing error evaluated using (58) for a second, fourth, sixth, and eighth order central-difference scheme, together with the subgrid term, computed using (77) for a fixed resolution, $k_m = 8$. It is seen that higher order schemes do lead to reduced levels of error. However, even with an eighth-order scheme, the subgrid contribution is dominated by numerical errors in about half of the wavenumber range. Plots similar to Fig. 4 for other values of k_m show the same qualitative behavior.

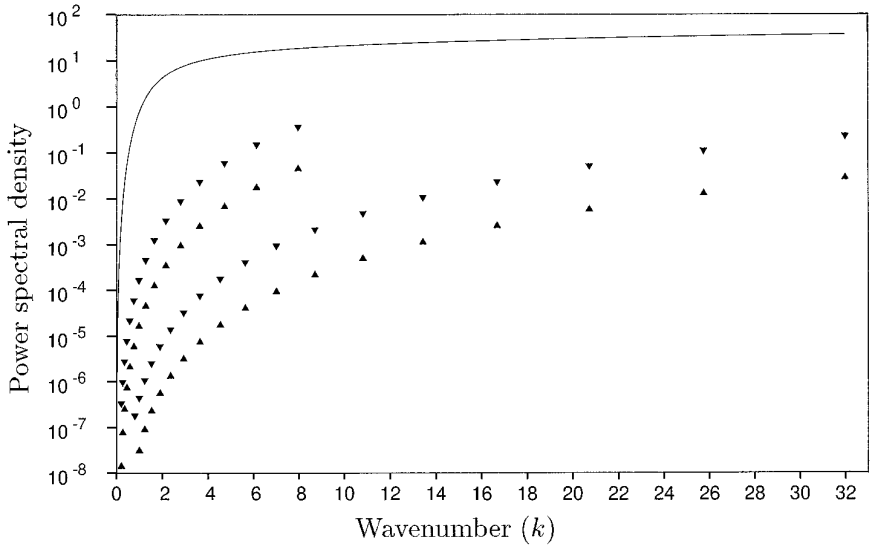

FIG. 2. The total nonlinear term (———) compared to the lower (▲) and upper (▼) bounds for the subgrid force for $k_m = 8$ and 32.

Figure 5 shows the corresponding comparison for the aliasing error. The aliasing error is seen to be substantially larger than the subgrid force. In general, increasing the order of a scheme has a relatively weak effect on the aliasing error and the effect is primarily in the high wavenumber region. This effect is in fact in the "reverse" direction, compared to the finite-differencing error. That is, the lowest pair of curves which correspond to a second-order scheme have the smallest aliasing error and the highest pair corresponding to an undealiased pseudo-spectral method have the largest. The aliasing errors for sixth- and eighth-order schemes are intermediate between the fourth and the pseudo-spectral; they have been omitted from Fig. 5 for clarity. The effect is, of course, quite easy to understand. In the one-dimensional problem, the aliasing part of the nonlinear term is multiplied by the modified wavenumber which approaches zero at the cutoff so that the aliasing error is also reduced to zero at k_m. In the three-dimensional problem a similar situation applies, except that the power spectrum does not actually go to zero because of the aver-

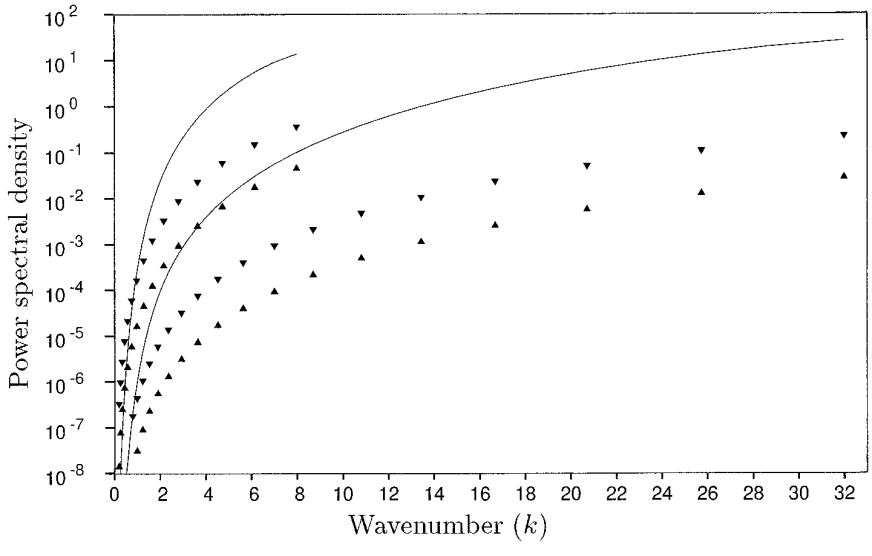

FIG. 3. The finite-differencing error of a second order scheme (———) compared to the lower (▲) and upper (▼) bounds for the subgrid force for $k_m = 8$ and 32.

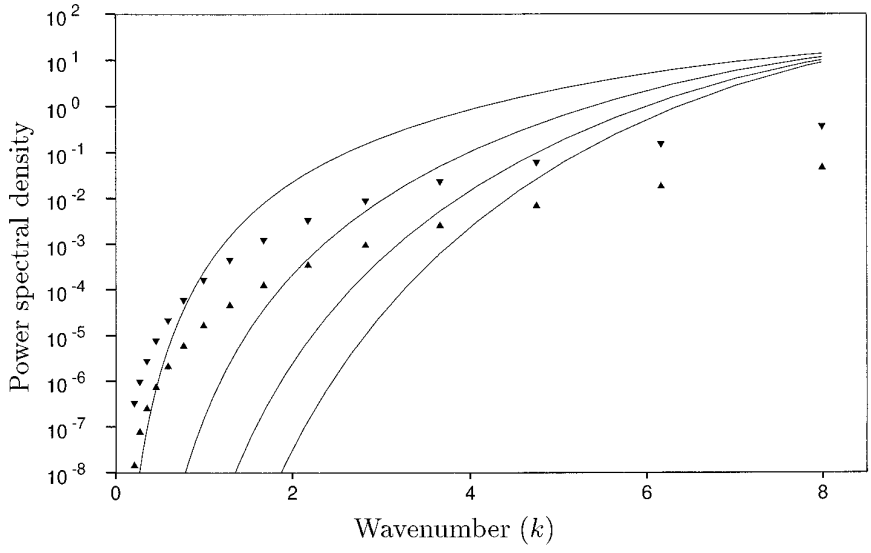

FIG. 4. Finite-differencing errors (———) compared to the lower (▲) and upper (▼) bounds of the subgrid force for $k_m = 8$. The numerical schemes considered are second (highest curve), fourth, sixth, and eighth (lowest curve) order central-differences.

aging over wavenumber shells. However, the aliasing error is reduced at high wavenumbers for central-difference schemes.

7.2. *Scaling Laws*

In this section, the dependence of some measure of "global error" on resolution, k_m, is investigated. An appropriate measure of the kind is

$$\sigma_* = \left[\int_0^{k_m} \mathscr{E}^{(*)}(k)\, dk\right]^{1/2}, \tag{81}$$

where "*" stands for "FD," "alias," "nl," or "sg," corresponding to the global finite-differencing error, aliasing error, total nonlinear term, or subgrid term, respectively. σ_* is closely related but not exactly equal to the rms value, which is given by the integral of the power spectrum over

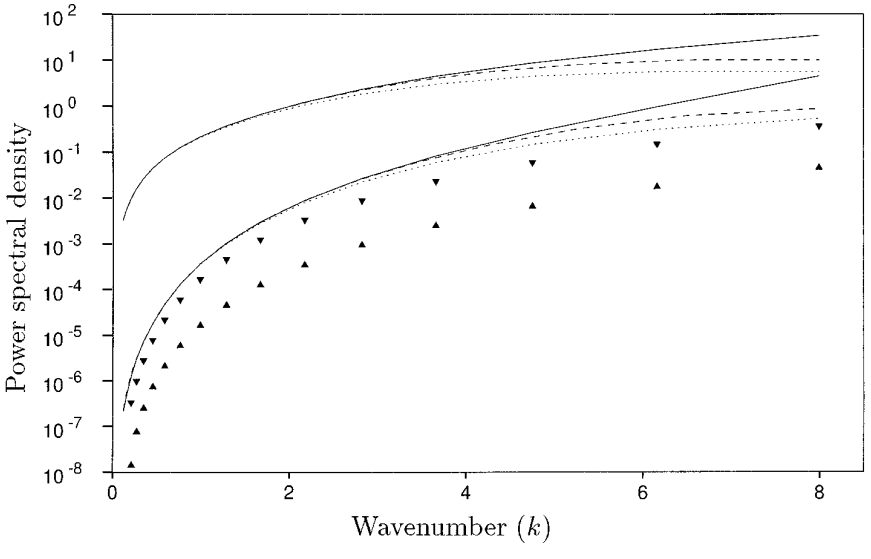

FIG. 5. The aliasing errror for a second-order central-difference method (···), a fourth-order central-difference method (---) and an underaliased pseudo-spectral method (———), compared to the lower (▲) and upper (▼) bounds for the subgrid force. Each method is represented by a pair of curves corresponding to the lower and upper bounds for the error.

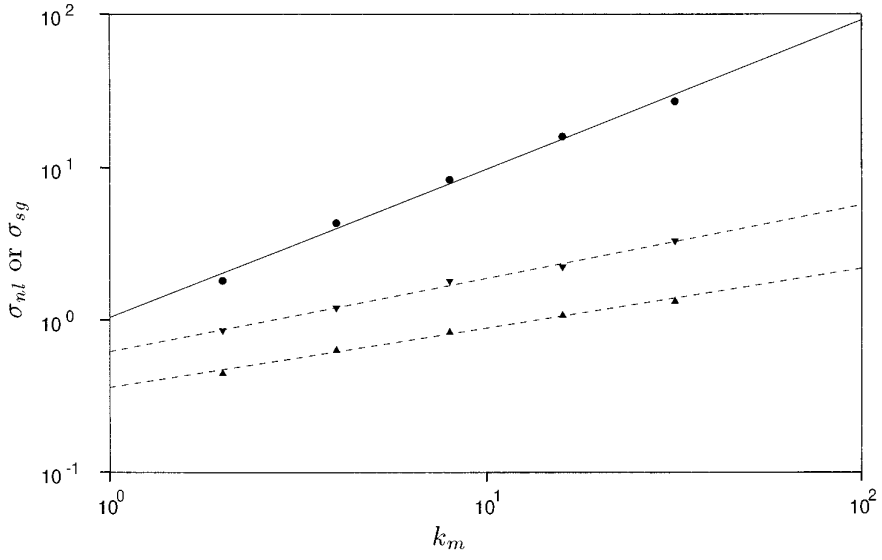

FIG. 6. Global measure of the total nonlinear term, $\sigma_{\rm nl}$ (●) and subgrid force, $\sigma_{\rm sg}$ (lower bound, ▲; upper bound, ▼) plotted as a function of the maximum resolved wavenumber, k_m. The lines represent power law fits obtained by the least-squares method.

the entire wavenumber range. The correspondence is not exact because the modes at the corners of the cube $[-k_m, k_m] \times [-k_m, k_m] \times [-k_m, k_m]$ outside of the inscribed sphere of radius k_m have not been included in the definition (81). Thus, σ_* is a lower bound of the true rms value. The σ_* can be evaluated as a function of k_m by numerically integrating the power spectra $\mathscr{E}^{(*)}(k)$ presented earlier.

Figure 6 shows the lower and upper bounds for the rms values of the subgrid force $\sigma_{\rm sg}$ as a function of k_m. The corresponding quantity for the total nonlinear term $\sigma_{\rm nl}$ is also shown for comparison. The subgrid contributions are seen to obey a power law. A least squares fit gives

$$\sigma_{\rm sg} = \begin{cases} 0.36\, k_m^{0.39} & \text{(lower bound)} \\ 0.62\, k_m^{0.48} & \text{(upper bound).} \end{cases} \tag{82}$$

The total nonlinear term also appears to follow a power law. A least squares fit in this case gives

$$\sigma_{\rm nl} = 1.04\, k_m^{0.97}. \tag{83}$$

The fitted curves (82) and (83) are shown in Fig. 6 as dashed and solid lines, respectively. Thus, the relative subgrid contribution is (roughly) $\sigma_{\rm sg}/\sigma_{\rm nl} \sim k_m^{-0.5}$; that is, the role of the subgrid model decreases at higher resolution. As an illustration, for an LES that resolves about a decade of scales beyond the energy peak, the rms value of the subgrid force, according to this formula, should be in the approximate range 11–19% of the rms value of the total force.

The following heuristic argument [16] is sometimes given for the scaling of the subgrid term. The subgrid stress is $\tau_{ij} = 2\nu_t S_{ij}$, where ν_t is the eddy-viscosity and S_{ij} is the rate of strain. The rate of dissipation $\varepsilon = \tau_{ij} S_{ij} = \nu_t |S|^2$ is a constant according to the classical Kolmogorov argument. Therefore, $|\tau_{ij}| \sim \nu_t |S| \sim \sqrt{\varepsilon \nu_t}$. Now, it seems reasonable to postulate that ν_t is the product of the grid-spacing, Δ, and the rms velocity of the subgrid eddies, $\sqrt{\langle u'^2 \rangle}$. The latter can be estimated from the Kolmogorov spectrum

$$\begin{aligned} \sqrt{\langle u'^2 \rangle} = \left[\int_{k_m}^{\infty} E(k)\, dk \right]^{1/2} &\sim \left[\int_{k_m}^{\infty} k^{-5/3}\, dk \right]^{1/2} \\ &\sim (k_m)^{-1/3} \sim \Delta^{1/3}. \end{aligned} \tag{84}$$

Thus, $\nu_t \sim \Delta \Delta^{1/3} \sim \Delta^{4/3}$ so that $|\tau_{ij}| \sim \sqrt{\varepsilon \nu_t} \sim \Delta^{2/3}$. The subgrid force, which is the derivative of τ_{ij} should then scale as $|\tau_{ij}|/\Delta \sim \Delta^{-1/3} \sim (k_m)^{1/3}$. The scaling exponent (0.4–0.5) in (82) is reasonably close to what this rough argument predicts. It should be noted that, even though the subgrid stress decreases with increasing resolution, its derivative, the subgrid force, actually increases.

Figure 7 shows the integrated value of the finite-differencing error, $\sigma_{\rm FD}$, plotted against k_m. There appears to be an asymptotic approach to a power law behavior for large k_m. A least squares power law fit to the last three data points gives

$$\sigma_{\rm FD} = k_m^{0.75} \times \begin{cases} 1.03 & \text{(order 2)} \\ 0.82 & \text{(order 4)} \\ 0.70 & \text{(order 6)} \\ 0.5 & \text{(order 8)} \\ 0 & \text{(spectral)} \end{cases} \tag{85}$$

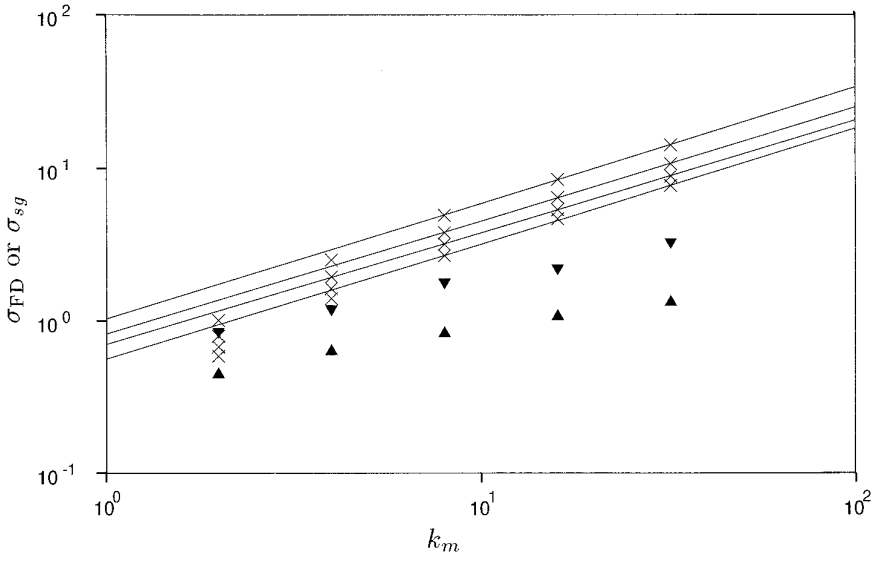

FIG. 7. Finite-differencing errors, σ_{FD} plotted as a function of the maximum resolved wavenumber k_m ($\times$) for central differencing schemes of order 2 (topmost), 4, 6, and 8 (lowermost). The solid lines are least-squares power law fits. Lower (▲) and upper (▼) bounds for the subgrid force σ_{sg} are also shown for comparison.

which are shown as solid lines in Figure 7. The subgrid terms σ_{sg} are also shown for comparison. It is significant that the exponent in the dependence of the integrated error on resolution in (85) turns out to be independent of the order of the scheme. A higher order scheme reduces the error only through a reduced prefactor multiplying the $\sim k_m^{0.75}$ term.

Figure 8 shows the integrated value of the aliasing error σ_{alias} plotted against k_m. The lines are power law fits to the data. Only the second-order scheme and the pseudo-spectral scheme without dealiasing is shown. The curves for the fourth, sixth, and eighth order schemes have intermediate positions and have been omitted for clarity. These fits are given by the following analytical expressions:

$$\sigma_{\mathrm{alias}} = \begin{cases} 0.90\, k_m^{0.46} & \text{(lower bound, undealiased pseudo-spectral)} \\ 2.20\, k_m^{0.66} & \text{(upper bound, undealiased pseudo-spectral)} \\ 0.46\, k_m^{0.41} & \text{(lower bound, second-order)} \\ 1.29\, k_m^{0.65} & \text{(upper bound, second-order).} \end{cases} \tag{86}$$

The important distinction from Fig. 7 is that here the curves are ''reversed.'' Thus, the lowest curve corresponds to the second-order scheme and the highest corresponds to an undealiased pseudo-spectral scheme. The subgrid term σ_{sg} is also shown for comparison. Of course, for a spectral scheme properly dealiased with the ''3/2-rule'' both the aliasing, as well as the finite-differencing, errors are identically zero.

8. DISCUSSIONS

The results of the above analysis may be summarized as follows. In large-eddy simulation, the net effect of the unresolved eddies on the resolved ones is represented by a subgrid model. The resulting equations, which are the Navier–Stokes equations augmented by an additional term, the subgrid force, is then solved numerically. In such a procedure the presumption is that the associated numerical errors are small compared to the subgrid model being used. To keep the analysis as simple as possible, isotropic turbulence in a ''box'' with periodic boundary conditions was considered together with a simple numerical method: an order n ($n = 2$ to 8) central-difference scheme with the nonlinear term in the divergence form. It was found that the most serious source of error is the aliasing error. The power spectrum of the aliasing error is significantly larger than the subgrid term and falls off less rapidly than the finite-differencing errors at low wavenumbers. Higher order schemes have the effect of increasing the aliasing error, although to a first approximation the aliasing error may be considered independent of the finite-difference scheme. The finite-differencing error for a second-order scheme also remains significantly larger than the subgrid term over most of the wavenumber range. The situation is improved by going to higher-order schemes. However, even for an

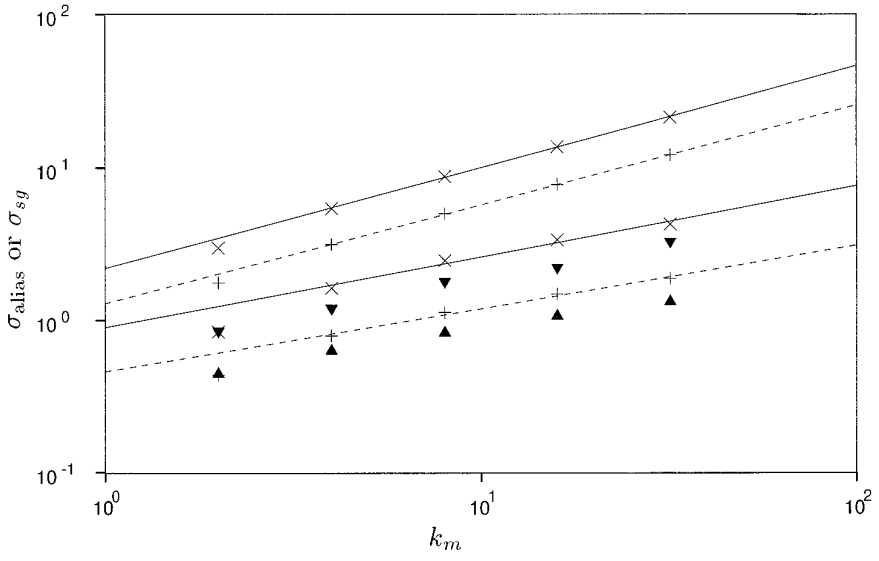

FIG. 8. Lower and upper bounds for the integrated aliasing error, σ_{alias}, for a second-order (+) and undealiased pseudo-spectral method (×). Solid and dashed lines are least-square power law fits. Lower (▲) and upper (▼) bounds for the integrated subgrid force σ_{sg} are also shown for comparison.

eighth-order scheme, the error is smaller than the subgrid term for only about half of the wavenumber range. An increase in grid resolution makes the errors increase faster than the subgrid force so that the situation cannot be improved by grid refinement alone as long as the cutoff, k_m, remains in the inertial range.

The analysis presented here is kinematic in nature in the sense that the departure of the Navier–Stokes operator from its ideal value was used to define the error. The effect of this error on the dynamics of the solution and ultimately on the prediction of statistical averages remain unknown. However, in the light of the present finding that numerical errors can be comparable to the subgrid term, a careful and systematic evaluation of the effect of finite-difference methods on turbulence simulations would seem essential. Such a study has recently been conducted by Kravchenko and Moin [17]. They used a channel flow pseudo-spectral code that uses B-splines in the wall normal direction and trigonometric basis functions in the homogeneous directions. By replacing the wavenumbers by the modified wavenumbers in the homogeneous directions they were able to mimic various finite difference schemes. Numerical experiments were run with various forms (divergence, rotational, skew-symmetric) of the nonlinear terms with or without "dealiasing". Aliasing errors in general were found to have a very serious effect on the simulation causing the flow to laminarize in some cases, as might be expected in the light of the present analysis. The effect of aliasing errors on the simulation as well as their size was found to depend strongly on both the form of the nonlinear term as well as the order of the scheme. Aliasing errors had the most serious effect for (undealiased) pseudo-spectral methods, a result also consistent with the present study. The effect of aliasing errors on numerical simulations have also been studied by [5, 18, 19] among others. In the light of the present analysis as well as the above studies, it is imperative that methods of reducing numerical errors in LES to acceptable levels be investigated. One method of achieving this goal is briefly discussed below.

In LES the Navier–Stokes equations are first "filtered" to remove all scales below some "filter-width," Δ_f. The resulting equations are then discretized on a grid of spacing Δ_g. In order that the smallest resolved scales be representable on the grid, it is required that $\Delta_g \leq \Delta_f$. In practice one most often assumes $\Delta_g = \Delta_f$, to minimize computational cost and accepts the consequence that the "marginal" eddies may not be well resolved. As a matter of fact, this distinction between Δ_g and Δ_f is often ignored and one speaks of "filter-width" and "grid-spacing" interchangably. However, if one expects to adequately resolve all scales up to "Δ_f" it is natural to require that "Δ_g" be several times smaller than "Δ_f." Thus, we are led to consider an LES with a filter-width Δ_f performed on a numerical grid of spacing $\Delta_g < \Delta_f$. Clearly, in any such computation all Fourier-modes between $k_m^f = \pi/\Delta_f$ and $k_m^g = \pi/\Delta_g$ must be held at very low amplitudes for, otherwise, these "contaminated" modes would soon destroy the accuracy of computation of the modes $(0, k_m^f)$ through nonlinear interactions. This might be achieved naturally by the effective "dissipation range" of the eddy-viscosity. This

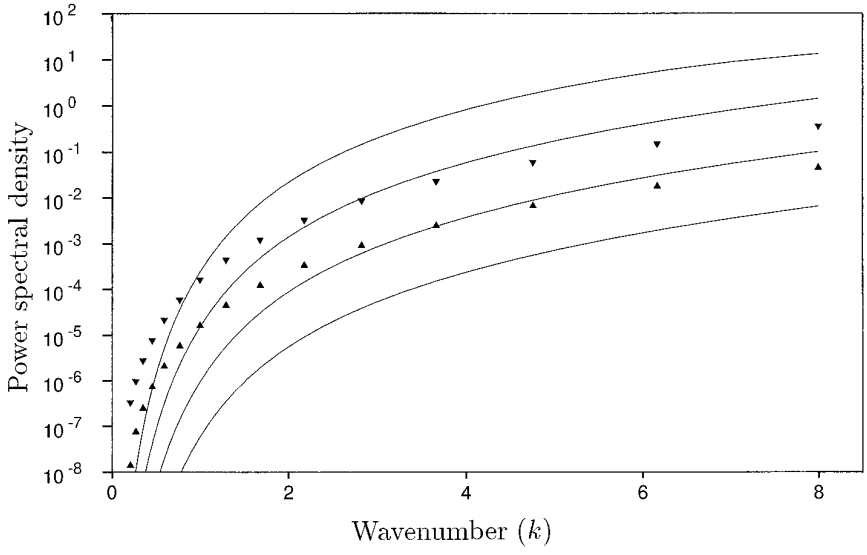

FIG. 9. The finite-differencing error (———) for a second-order central-difference scheme with $\Delta_f = N\Delta_g$ for $N = 1$ (uppermost curve), 2, 4, and 8 (lowermost curve). The lower (▲) and upper (▼) bounds for the subgrid force are shown for comparison. $k_m^f = 8$ is held fixed.

may also be achieved by replacing the discretization (2) of the Navier–Stokes equations by the alternative [20]

$$\frac{\partial u_i}{\partial t} = -\frac{\delta}{\delta x_j}\mathscr{F}[u_i u_j] - \frac{\delta \mathscr{F}[P]}{\delta x_i} - \frac{\delta \mathscr{F}[T_{ij}^M]}{\delta x_j} + \nu \frac{\delta}{\delta x_k}\frac{\delta}{\delta x_k} u_i, \tag{87}$$

where $\mathscr{F}[\,]$ represents a suitably designed filtering operation that reduces the amplitudes of all modes in the range (k_m^f, k_m^g) to zero or very small values. Such compact filters for finite difference schemes that are close to a sharp low pass filter in Fourier space were first considered by Lele [21] and they have been used in the present context by Lund [20]. The finite-differencing operator $\delta/\delta x_j$ is on the finer grid Δ_g. The effect of this modification is easy to investigate in the present formalism. Thus, for a second-order method, the "Δ" in the expression for the modified wavenumber need simply be replaced with Δ_g. Figure 9 shows the result of such a computation for a second-order central-difference method with $\Delta_g = \Delta_f/N$, where $N = 1$, 2, 4, and 8 for a fixed $k_m^f = 8$. It is seen that with $N = 8$, the finite-differencing error is about one or two orders of magnitude below the subgrid term throughout the wavenumber range from $k = 0$ to $k = k_m^f = 8$. However, taking $\Delta_g = \Delta_f/8$ increases the number of grid points by a factor of $8^3 = 512$ and the total computational cost (if the time-step, Δt is limited by the CFL condition so that $\Delta t \sim \Delta_g$) by a factor of $8^4 = 4096$. It may therefore be advisable to use, instead, a higher order scheme, in conjunction with a grid that is finer than the filter-width. In Fig. 10, Δ_g has been fixed at $\Delta_f/2$ and the spectra of finite-differencing errors is plotted for a second, fourth, and eighth order scheme. It is seen that for an eighth-order scheme the finite-differencing error is several orders of magnitude below the subgrid term. The increase in computational cost due to the refined grid is a factor of $2^4 = 16$. Implementation of an eighth-order scheme would also carry a penalty in terms of added cost. However, in view of the vastly increased accuracy, the additional cost may be justified. In addition to reducing the finite-differencing error, the filtering scheme (87) completely removes the aliasing error. This is because modes $\mathbf{k}'$ and $\mathbf{k}''$ that "alias" to a mode $\mathbf{k}$ must satisfy the relation $\mathbf{k}' + \mathbf{k}'' - \mathbf{k} = \mathbf{a}$, where $\mathbf{a}$ is a member of the "reciprocal lattice" Λ. The magnitude of any component of the vector on the left of this equation can be at most k_m^f so that the left-hand side cannot exceed $3k_m^f$. Since at least one component on the right-hand side is $2k_m^g$ or larger, the equation cannot be satisfied if $3k_m^f < 2k_m^g$; that is, if $\Delta_g < (2/3)\Delta_f$ there cannot be any aliasing errors. This is, of course, the justification for the well-known "3/2 dealiasing rule" [13].

In conclusion, a method of analysis of numerical errors in finite-difference implementations of the Navier–Stokes equations was presented that takes into account the continuum of length scales present in turbulence. In the case of LES with the grid cutoff in the inertial range, the resulting numerical errors were shown to be quite large, compared to the subgrid force for finite difference schemes up to eighth-order accurate, irrespective of the grid resolution. However, the errors can be brought under control by im-

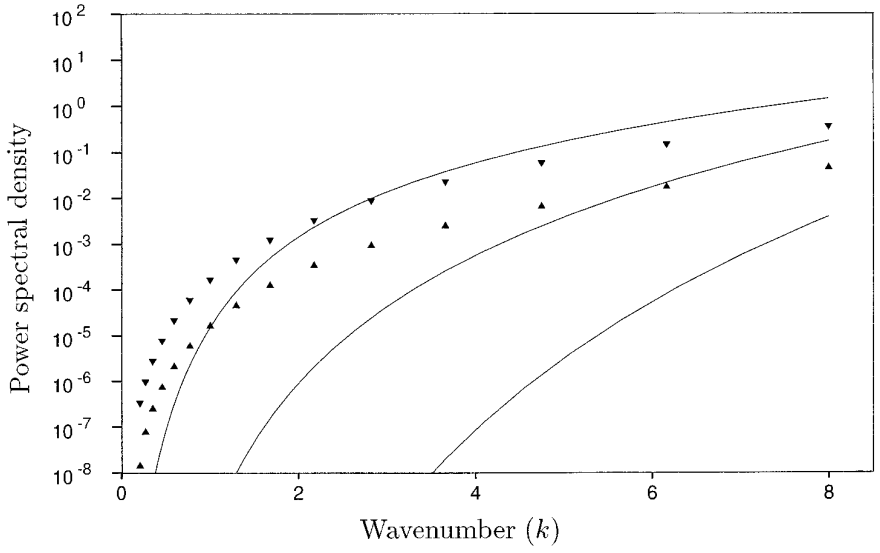

FIG. 10. The finite-differencing error (———) for $\Delta_f = 2\Delta_g$ for a second (uppermost), fourth and eighth (lowermost) order central-difference scheme. The lower (▲) and upper (▼) bounds for the subgrid force are shown for comparison. $k_m^f = 8$ is held fixed.

plementing the LES with a filter-width that is greater than the grid-width combined with some filtering scheme that sharply reduces any fluctuations on a scale shorter than the filter-width. Thus, an eighth-order central-difference scheme combined with a filter to grid width ratio of 2 has numerical errors that are several orders of magnitude smaller than the subgrid force throughout the entire wavenumber range of interest. The analytical formulas developed in this paper can also be used to analyze numerical errors in DNS. Further, these techniques can be used to study more sophisticated numerical schemes than the ones considered here. The analysis with suitable modifications can be applied to other simple geometries such as channel flow. The requirement that the turbulence be isotropic can be relaxed to simply a requirement of homogeneity in one or more directions.

APPENDIX: EVALUATION OF THE INTEGRAL IN SECTION 4

We will evaluate the integral

$$\begin{aligned} J_{mpnq}(\mathbf{k}) &\equiv 8\pi k^2 \int \Phi^*_{mp}(\mathbf{k}')\Phi^*_{nq}(\mathbf{k}-\mathbf{k}')\, d\mathbf{k}' \\ &= \frac{k^2}{2\pi}\int\int \frac{E(P)E(Q)}{P^4Q^4}\,[P^2Q^2\delta_{mp}\delta_{nq} - P_mP_qQ^2\delta_{nq} \\ &\quad - Q_nQ_qP^2\delta_{mp} + P_mP_pQ_nQ_q] \\ &\quad \delta(\mathbf{P}+\mathbf{Q}-\mathbf{k})\, d\mathbf{P}\, d\mathbf{Q}. \end{aligned} \tag{88}$$

It clearly suffices to evaluate

$$\begin{aligned} \mathcal{I}_{mpnq} &\equiv \frac{k^2}{2\pi}\int\int \frac{E(P)E(Q)}{P^4Q^4} \\ &\quad P_mP_pQ_nQ_q\delta(\mathbf{P}+Q-\mathbf{k})\, d\mathbf{P}\, d\mathbf{Q} \end{aligned} \tag{89}$$

since, from inspection of the definition of J_{mpnq}, it follows that

$$J_{mpnq} = \mathcal{I}_{aabb}\delta_{mp}\delta_{nq} - \mathcal{I}_{mpaa}\delta_{nq} - \mathcal{I}_{aanq}\delta_{mp} + \mathcal{I}_{mpnq}. \tag{90}$$

If the domain of integration in (89) is infinite for each of the variables **P** and **Q** or if the domain has spherical symmetry, then clearly the result of the integration would be some combination of the components of **k**, together with some numerical coefficients. Further, the integral $\mathcal{I}_{mpnq}$ is symmetric under the following permutations of indices $m \leftrightarrow p$, $n \leftrightarrow q$, as well as $(m,p) \leftrightarrow (n,q)$. The most general rank four tensor of this kind that can be constructed from the wave vector **k** is

$$\begin{aligned} \mathcal{I}_{mpnq} &= A\delta_{mp}\delta_{nq} + B(\delta_{mn}\delta_{pq} + \delta_{pn}\delta_{mq}) \\ &\quad + C\left(\frac{k_mk_p}{k^2}\,\delta_{nq} + \frac{k_nk_q}{k^2}\,\delta_{mp}\right) + D\,\frac{k_mk_pk_nk_q}{k^4}, \end{aligned} \tag{91}$$

where A, B, C, and D are scalar functions of k. It should be noted that the form (91) is true only for domains that have spherical symmetry. For a more general domain (such as a cube) the integral would depend not only on **k** but on some other vector **A** characterizing the orientation of the domain. In that case Eq. (91) would no longer be true and our method of evaluating the integral would not be

valid. The method can be modified by including in (91) appropriate combinations of **A** and **k** but the analysis would then be considerably more complicated. Let us define the four integrals $I_1 = \mathcal{I}_{aabb}$, $I_2 = \mathcal{I}_{abab}$, $I_3 = (k_b k_c/k^2)\,\mathcal{I}_{aabc}$, and $I_4 = (k_a k_b k_c k_d/k^4)\,\mathcal{I}_{abcd}$. Then, on contraction of (91), we have

$$9A + 6B + 6C + D = I_1 \tag{92}$$

$$3A + 12B + 2C + D = I_2 \tag{93}$$

$$3A + 2B + 4C + D = I_3 \tag{94}$$

$$A + 2B + 2C + D = I_4 \tag{95}$$

which on inversion gives

$$A = \tfrac{1}{16}[7I_4 - 10I_3 - 2I_2 + 5I_1] \tag{96}$$

$$B = \tfrac{1}{16}[-3I_4 + 2I_3 + 2I_2 - I_1] \tag{97}$$

$$C = \tfrac{1}{16}[-15I_4 + 18I_3 + 2I_2 - 5I_1] \tag{98}$$

$$D = \tfrac{1}{16}[45I_4 - 30I_3 - 6I_2 + 7I_1]. \tag{99}$$

On substituting these expressions in (91) we get $\mathcal{I}_{mpnq}$ which gives, upon substitution in (90), the expression

$$\begin{aligned} J_{mpnq}(\mathbf{k}) = {} & F_1(k)\delta_{mp}\delta_{nq} + F_2(k)(\delta_{mn}\delta_{pq} + \delta_{pn}\delta_{mq}) \\ & + F_3(k)\left[\frac{k_m k_p}{k^2}\,\delta_{nq} + \frac{k_n k_q}{k^2}\,\delta_{mp}\right] \\ & + F_4(k)\,\frac{k_m k_p k_n k_q}{k^4}, \end{aligned} \tag{100}$$

where

$$F_1(k) = \tfrac{1}{16}[7I_4 + 6I_3 - 2I_2 + 5I_1] \tag{101}$$

$$F_2(k) = \tfrac{1}{16}[-3I_4 + 2I_3 + 2I_2 - I_1] \tag{102}$$

$$F_3(k) = \tfrac{1}{16}[-15I_4 - 6I_3 + 2I_2 + 3I_1] \tag{103}$$

$$F_4(k) = \tfrac{1}{16}[45I_4 - 30I_3 - 6I_2 + 7I_1]. \tag{104}$$

It only remains to evaluate I_1, I_2, I_3, and I_4. We have

$$\begin{aligned} I_1 = \mathcal{I}_{aabb} &= \frac{k^2}{2\pi}\int\int \frac{E(P)E(Q)}{P^2Q^2}\,\delta(\mathbf{P} + \mathbf{Q} - \mathbf{k})\,d\mathbf{P}\,d\mathbf{Q} \\ &= \frac{k^2}{2\pi}\int \frac{E(P)E(|\mathbf{k} - \mathbf{P}|)}{P^2|\mathbf{k} - \mathbf{P}|^2}\,d\mathbf{P}. \end{aligned} \tag{105}$$

Let us introduce spherical polar coordinates in the space **P** with the z-axis oriented along the vector **k**. Then,

$$I_1 = \frac{k^2}{2\pi}\int_0^\infty dP \int_0^\pi d\theta\, \frac{E(P)E(\sqrt{k^2 + P^2 - 2kP\cos\theta})}{P^2(k^2 + P^2 - 2kP\cos\theta)}\,2\pi P^2 \sin\theta. \tag{106}$$

Let us replace P by the new variable $\xi = P/k$ and θ by $\eta = \sqrt{1 + \xi^2 - 2\xi\cos\theta}$. Then,

$$I_1 = k\int_0^\infty d\xi \int_{|\xi-1|}^{\xi+1} d\eta\, \frac{E(k\xi)E(k\eta)}{\xi\eta}. \tag{107}$$

Similarly, one obtains

$$I_2 = k\int_0^\infty d\xi \int_{|\xi-1|}^{\xi+1} d\eta\, E(k\xi)E(k\eta)\left[\frac{(1 - \xi^2 - \eta^2)^2}{4\xi^3\eta^3}\right], \tag{108}$$

$$I_3 = k\int_0^\infty d\xi \int_{|\xi-1|}^{\xi+1} d\eta\, E(k\xi)E(k\eta)\left[\frac{(1 - \xi^2 - \eta^2)^2}{4\xi^3\eta}\right], \tag{109}$$

$$I_4 = k\int_0^\infty d\xi \int_{|\xi-1|}^{\xi+1} d\eta\, E(k\xi)E(k\eta)\left[\frac{\{1 - (\xi^3 - \eta^2)^2\}^2}{16\xi^3\eta^3}\right]. \tag{110}$$

ACKNOWLEDGMENTS

I thank Professor Parviz Moin for his encouragement and constructive suggestions (in particular, for suggesting the use of the Von-Karman spectrum in Section 7). I am also grateful to all (in particular, Professor Joseph Keller, Professor Robert Moser, and Dr. Karim Shariff) who read the evolving manuscript and shaped the final version through their insightful comments. The discussion in Section 8 is partly motivated by a suggestion from Dr. Thomas Lund. The support of the Center for Turbulence Research (Stanford & NASA Ames) in the form of a research fellowship is gratefully acknowledged. During the final preparation of this manuscript I was supported by the Center for Nonlinear Studies (Los Alamos National Laboratory) as a postdoctoral fellow.

REFERENCES

1. R. Rogallo and P. Moin, *Annu. Rev. Fluid Mech.* **16,** 99 (1984).
2. C. Chu, *Adv. in Applied Mech.* **18,** 285 (1978).
3. G. Batchelor, *Proc. Cambridge Philos. Soc.* **47,** 359 (1951).
4. G. Batchelor, *The Theory of Homogeneous Turbulence* (Cambridge Univ. Press, Cambridge, United Kingdom, 1953).
5. G. Blaisdell, E. Spyropoulos, and J. Qin, *Appl. Numer. Math.*, submitted.
6. H. Lomax, Lecture notes, Stanford University.
7. W. Gear, *Numerical Initial Value Problems in Ordinary Differential Equations* (Prentice–Hall, Englewood Cliffs, NJ, 1971).
8. E. Isaacson and H. Keller, *Analysis of Numerical Methods* (Wiley, New York, 1966).
9. G. Helmberg, *Introduction to Spectral Theory in Hilbert Space* (North-Holland, Amsterdam London, 1969).

10. W. Jones and N. March, *Theoretical Solid State Physics, Vol. 1: Perfect Lattices in Equilibrium* (Wiley-Interscience, London, 1973).
11. M. Lesieur, *Turbulence in Fluids* (Kluwer Academic, Dordrecht, 1987).
12. R. Vichnevetsky and J. Bowles, *Fourier Analysis of Numerical Approximations of Hyperbolic Equations* (SIAM, Philadelphia, 1982).
13. C. Canuto, M. Hussaini, A. Quarteroni, and T. Zang, *Spectral Methods in Fluid Dynamics* (Springer-Verlag, Berlin, 1988).
14. R. Rogallo, NASA Tech. Memo TM81315, 1981 (unpublished).
15. A. Monin and A. Yaglom, *Statistical Fluid Mechanics, Vol. 2* (MIT Press, Cambridge, MA, 1979).
16. H. Tennekes and J. L. Lumley, *A First Course in Turbulence* (MIT Press, Cambridge, MA, London, 1983).
17. A. Kravchenko and P. Moin, (preprint) (1995).
18. T. Zang, *Appl. Numer. Math.* **7,** 27 (1991).
19. R. Moser, P. Moin, and A. Leonard, *J. Comput. Phys.* **52,** 524 (1982).
20. T. Lund, unpublished.
21. S. Lele, *J. Comput. Phys.* **103,** 16 (1992).